

Early human impact on soils and hydro-sedimentary systems: multi-proxy geoarchaeological analyses from La Narse de la Sauvetat (France)

Journal:	<i>The Holocene</i>
Manuscript ID	HOL-19-0169.R2
Manuscript Type:	Paper
Date Submitted by the Author:	n/a
Complete List of Authors:	Mayoral, Alfredo; Clermont Auvergne University, GEOLAB UMR 6042; Institut Catala d'Arqueologia Classica Granai, Salome; GéoArchÉon; UMR 8591 Develle, Anne-Lise; UMR 5204 EDYTEM Peiry, Jean-Luc; Clermont Auvergne University; UMR 5204 EDYTEM Miras, Yannick; Histoire naturelle de l'Homme préhistorique, UMR 7194 CNRS; Clermont Auvergne University, GEOLAB UMR 6042 Couderc, Florian; UMR 5608 TRACES Vernet, Gérard; GEOLAB UMR 6042-INRAP Berger, Jean-François; UMR 5600, CNRS
Keywords:	Geoarchaeology, Palaeoenvironment, Socio-environmental interaction, Anthropogenic impact, Holocene, Limagne
Abstract:	<p>We analyzed the Late Holocene pedo-sedimentary archives of La Narse de la Sauvetat, a hydromorphic depression in the southern Limagne plain (central France), where chronologically accurate studies are scarce. The multi-proxy geoarchaeological and palaeoenvironmental analysis of two cores from different areas of the basin was carried out through sedimentological, geochemical, micromorphological and malacological investigations. Integration of these datasets supported by a robust radiocarbon-based chronology allowed discussion of socio-environmental interactions and anthropogenic impacts from Late Neolithic to Early Middle Ages. Until the Middle Bronze Age, there was no clear evidence of anthropogenic impact on soils and hydro-sedimentary dynamics of the catchment, but two peaks of high alluvial activity probably related to the 4.2 and 3.5 kyr. BP climate events were first recorded in Limagne. Significant anthropogenic impacts started in the Late Bronze Age with increased erosion of the surrounding volcanic slopes. However, a major threshold was reached c. 2600 cal BP with a sharp increase in the catchment erosion interpreted as resulting from strong anthropogenic environmental changes related to agricultural activities and drainage. This implies an anthropogenic forcing on soils and hydro-sedimentary systems much earlier than was usually considered in Limagne. These impacts then gradually increased during Late Iron Age and Roman periods, but environmental effects were certainly contained by progress in agricultural management. Late Antiquity environmental changes are consistent with regional trend to drainage deterioration in lowlands, but</p>

1
2
3
4
5
6
7
8
9
10
11
12
13
14
15
16
17
18
19
20
21
22
23
24
25
26
27
28
29
30
31
32
33
34
35
36
37
38
39
40
41
42
43
44
45
46
47
48
49
50
51
52
53
54
55
56
57
58
59
60

	marked asynchrony in this landscape change suggests that societal factors implying differential land management were certainly predominant here.



Early human impact on soils and hydro-sedimentary systems: multi-proxy geoarchaeological analyses from La Narse de la Sauvetat (France)

MAYORAL, Alfredo* (1); GRANAI, Salomé (2); DEVELLE, Anne-Lise (3); PEIRY, Jean-Luc (4); MIRAS, Yannick (5); COUDERC, Florian (6); VERNET, Gérard (7); BERGER, Jean-François (8)

1. Université Clermont Auvergne, CNRS, GEOLAB, F-63000 Clermont-Ferrand, France & Catalan

Institute of Classical Archaeology, Pl. Rovellat s/n, 43003 Tarragona, Spain.

2. GéoArchÉon, 30 Rue de la Victoire, 55210 Vigneulles-lès-Hattonchâtel & CNRS, Université Paris 1,

UPEC. UMR8591, Laboratoire de Géographie Physique : Environnements Quaternaires et Actuels, 1

place Aristide Briand, 92195 Meudon, France

3. UMR 5204 EDYTEM, Université Savoie Mont Blanc, CNRS, 7337 Le Bourget du Lac, France

4. Université Clermont Auvergne, F-63000 Clermont-Ferrand & CNRS, EDYTEM, F-73000 Chambéry, France

5. CNRS, UMR7194, Histoire Naturelle de l'Homme Préhistorique, Département de Préhistoire,

Muséum National d'Histoire Naturelle, Institut de Paléontologie Humaine, Paris, France & Université

Clermont Auvergne, CNRS, GEOLAB, F-63000 Clermont-Ferrand, France

6. UMR 5608 TRACES, Université Toulouse 2 Jean Jaurès, CNRS, Toulouse, France

7. Université Clermont Auvergne, CNRS, INRAP, GEOLAB, F-63000 Clermont-Ferrand, France

8. CNRS, UMR 5600, EVS-IRG & Université Lyon 2, Lyon, France

*corresponding author : alfredo.mayoral@uca.fr

Abstract: We analyzed the Late Holocene pedo-sedimentary archives of La Narse de la Sauvetat, a hydromorphic depression in the southern Limagne plain (central France), where chronologically

accurate studies are scarce. The multi-proxy geoarchaeological and palaeoenvironmental analysis of two cores from different areas of the basin was carried out through sedimentological, geochemical, micromorphological and malacological investigations. Integration of these datasets supported by a robust radiocarbon-based chronology allowed discussion of socio-environmental interactions and anthropogenic impacts from Late Neolithic to Early Middle Ages. Until the Middle Bronze Age, there was no clear evidence of anthropogenic impact on soils and hydro-sedimentary dynamics of the catchment, but two peaks of high alluvial activity probably related to the 4.2 and 3.5 kyr. BP climate events were first recorded in Limagne. Significant anthropogenic impacts started in the Late Bronze Age with increased erosion of the surrounding volcanic slopes. However, a major threshold was reached c. 2600 cal BP with a sharp increase in the catchment erosion interpreted as resulting from strong anthropogenic environmental changes related to agricultural activities and drainage. This implies an anthropogenic forcing on soils and hydro-sedimentary systems much earlier than was usually considered in Limagne. These impacts then gradually increased during Late Iron Age and Roman periods, but environmental effects were certainly contained by progress in agricultural management. Late Antiquity environmental changes are consistent with regional trend to drainage deterioration in lowlands, but marked asynchrony in this landscape change suggests that societal factors implying differential land management were certainly predominant here.

Keywords: Geoarchaeology, Palaeoenvironment, Socio-environmental interactions, Anthropogenic impact, Holocene, Limagne

1-Introduction

Middle Holocene is now generally considered as the beginning of anthropogenic impact on natural systems, which becomes gradually stronger and more generalized during the Late Holocene (Crutzen & Stoermer, 2000; Ellis et al., 2017; Nichols & Gogineni, 2018; Ruddiman et al., 2015; Ruddiman, 2018). From a geomorphological perspective, the crucial step is the generalized and intensive anthropogenic modification of geomorphic processes, such as soil erosion, hydro-sedimentary

1
2
3 47 system forcing and pronounced development of anthropogenic landforms (Brown et al., 2016;
4
5 48 Goudie and Viles, 2016; Walsh et al., 2019).
6
7

8 49 In north-western Europe, this threshold appeared to occur in the third millennium BP (Dotterweich,
9
10 50 2013; Ellis et al., 2013; Notebaert, Berger, & Brochier, 2014; Ruddiman, 2003). While the forcing of
11
12 51 geomorphological processes in Roman times or at the end of the Iron Age is now accepted, some
13
14 52 authors argue that it could have occurred centuries earlier (e.g. Dreibrodt et al., 2010; Gebhardt,
15
16 53 Occhietti, & Fechner, 2014; Houben et al., 2012; Lang, 2003; Notebaert & Berger, 2014), in
17
18 54 connection with the development of a centralization and complexification phenomenon sometimes
19
20 55 qualified as “proto-urban” in central-western Europe (Fernández-Götz, 2018).
21
22
23

24
25 56 However, there are still some key open questions as the rates and thresholds in the broadly
26
27 57 increasing pace of anthropogenic impacts, or the relative contribution and interactions between
28
29 58 anthropogenic and climatic drivers. Spatial and temporal variability of anthropogenic impacts and
30
31 59 associated geomorphological responses, and a general scarcity of high-resolution, continuous and
32
33 60 robust datasets are amongst the main difficulties (Brown et al., 2013; 2016). Indeed, some areas such
34
35 61 as the Rhône valley in SE France are extensively studied (e.g. Berger, Shennan, & Woodbridge, 2019),
36
37 62 whereas other neighboring areas suffer from a dearth of analysis, poor data resolution or other
38
39 63 issues making a regional synthesis and discussion problematic.
40
41
42

43 64 Our work aimed to contribute to this scientific challenge providing new data in the Limagne plain
44
45 65 (central France) where even recent Holocene palaeoenvironmental and geoarchaeological research
46
47 66 often lacked chronological accuracy. This lack of chronological accuracy has hindered proper
48
49 67 discussion of socio-environmental interactions during critical protohistoric periods, despite abundant
50
51 68 studies conducted since the 2000s (Ballut, 2001; Macaire et al., 2010; Trément, 2007a; Trément,
52
53 69 2011; Vernet, 2013). The main objective of this study was therefore to bring out new multi-proxy
54
55 70 palaeoenvironmental and geoarchaeological data at high chronological resolution in Limagne, and
56
57
58
59
60

71 subsequently use them to discuss interactions of human activities with natural landscapes, especially
72 with soils and hydro-sedimentary system of the catchment, as well as local vegetation and hydrology.
73 We focused on a hydromorphic depression called La Narse de la Sauvetat located in the marly
74 lowlands of the southern Limagne, surprisingly neglected by palaeoenvironmentalists until recently.
75 Since 2014, first preliminary works detected particularly high potential for palaeoenvironmental
76 studies, encouraging further research (Mayoral et al., 2018). The basin is a flat depression with a W-E
77 elongated shape (2km x 800m approx.) and a surface of c. 1,2 km², dug in the Cenozoic calcareous
78 rocks of southern Limagne lowlands (Fig. 1).

79 In this area, the so-called *Limagne des Buttes*, incision of the drainage network after Miocene and
80 Pliocene volcanism (Nehlig et al., 2003) gradually created inverted volcanic reliefs from the basaltic
81 lava flows and domes (500 to 800 masl.), which now dominate the eroded sedimentary lowlands
82 (300-400 masl.). The slopes of these volcanic reliefs are covered by sedimentary or volcano-
83 sedimentary colluvium, sometimes with decametric thickness, and are affected by mass movements
84 and landslides (Greffier et al., 1980). Lowlands around the basin have a gentle topography, with
85 some structural reliefs in marls and limestones. La Narse de la Sauvetat catchment (c. 16 km²) is
86 therefore limited by volcanic plateaus and domes at the East and West (Puy de Corent, Puy de Saint-
87 Sandoux and Puy de Peyronère), a Pleistocene residual terrace of the Allier river to the North, and
88 small structural mounds to the South (Fig. 1B-C).

89 Water and sediment fluxes come mainly from westward colluvial slopes (Puy de Saint-Sandoux, Puy
90 de Peyronère), concentrated in several small flat valleys and are finally directed to the bottom of the
91 depression to the east (min. 368 masl.). The basin is naturally closed by a topographic threshold in its
92 eastern border and is therefore disconnected from drainage network, causing development of dark
93 hydromorphic soils with isohumic/vertic features which are nowadays artificially drained and
94 cultivated (see Fig. 1). Climate in the area is oceanic to semi-continental with cold and relatively dry
95 winters, and hot and stormy summers (Joly et al., 2010). Soils of the catchment include a variety of

96 brown soils on volcanic and/or calcareous materials, colluvial soils and regosoils on marls, gleyic
97 alluvial soils, and the aforementioned hydromorphic soils in the depressions (Bornand et al., 1968,
98 see Fig. 1D).

99 First research works provided supplementary geomorphological data on the nature of the basin and
100 its main phases of morpho-stratigraphic and pedo-sedimentary evolution (Mayoral et al., 2018). A
101 6m-thick alluvio-colluvial sedimentary infilling was investigated through hand auger cross-sections
102 (Fig. 2). Alluvial sedimentary dynamics have shown that La Narse de la Sauvetat was a palaeovalley
103 connected to local drainage from the Upper Pleistocene until the mid-Holocene period, when a
104 massive landslide formed the topographic threshold blocking its eastern outlet (see Fig. 1). Sudden
105 damming of the valley temporarily formed a lake, ultimately recaptured by headward erosion. The
106 drainage network remained nevertheless disturbed and poorly hierarchized and consequently the
107 area became an hydromorphic plain after c. 4850 cal BP, with palustrine and lacustrine phases until
108 its drainage in 1768 AD (Daugas and Tixier, 1977; Mayoral et al., 2018).

109 The basin is also situated within the rich protohistoric archaeological context of the Limagne plain,
110 with a particularly dense and well-known record from the Neolithic to the Roman period (Provost
111 and Mennessier-jouannet, 1994; Vallat, 2002). However, at a local scale the neighboring hilltop site
112 of the Puy de Corent, with multi-period occupations (Fig. 1C) crucial for territorial structuring from
113 the Neolithic to the Iron Age, has been the focus of almost all the research and findings. As a
114 consequence of this research bias, archaeological discoveries are rather scarce in the lowlands
115 surrounding La Narse de la Sauvetat basin. In general the Neolithic is poorly known in the lowlands
116 due to the lack of findings, however in the Puy de Corent developed settlements are known
117 especially in the second part of the Middle Neolithic (Poux et al., 2018). Most phases of the Bronze
118 Age are also poorly documented in the study area, however during the Middle Bronze Age a small
119 occupation is noted (Pranly, Fig. 1C). By contrast, extended settlements develop at Corent during the
120 Middle and the Late Bronze Age, and also during the Early Iron Age (Milcent et al., 2014; Poux et al.,

2018). During the latter period, a small site is also known in the lowlands (Les Orneufs, Fig. 1C). The area is especially known for the Late Iron Age (La Tène) extensive *oppidum* of Corent (Poux, 2012; Poux et al., 2018), however lowlands around La Narse de la Sauvetat again lack archaeological remains for this period. The only phase with abundant archaeological remains in la Sauvetat plain is the Roman era, as a secondary agglomeration develops at Corent. Several sites are documented around La Narse basin, including farms, a sanctuary and an extensive *villa*, indicating an intense exploitation of the area (Simon et al., 2017; Vallat, 2002).

With a view to fully use the set of palaeoenvironmental records of this sedimentary archive from the second part of the Holocene, we present here a multi-proxy geoarchaeological and palaeoenvironmental analysis of the upper infilling of the basin, broadly covering 3800 yr. between the Late Neolithic and the early Middle Ages (5000 to 1200 cal BP). Sedimentological, geochemical, micromorphological and malacological investigations were performed on two cores and supported by AMS radiocarbon dating. Results were here synthetized and discussed with other regional climate and palaeoenvironmental data for each archaeological period between the Late Neolithic and the early Middle Ages, in order to provide a more comprehensive perspective of socio-environmental interaction and human forcing of natural systems since the Mid-Holocene.

Figure 1. A) Location of study area, black line delineates Auvergne region; B) General view of study area from the summit of the Puy de Corent (location: see Fig. 1C, view direction: ESE). La Narse hydromorphic basin and its catchment are indicated with white and red dashed lines respectively. Light blue dashed line indicates hypothetical position of former river course (Pleistocene and Early Holocene), from cross sections and current topography (see Mayoral et al., 2018); C) Geomorphological sketch of la Narse de la Sauvetat catchment (modified from Mayoral et al., 2018) ; D) Main soils of the catchment (red dashed line) following Bornand et al., 1968 : a) lithosols and brown soils on basalts ; b) Calcareous and calcic brown soils on marls and basaltic colluvium ; c) Colluvial soils and regosols on marls and platy limestone ; d)

146 Calcareous brown soils on gentle slopes ; e) Clayey grey soils of marly depressions, hydromorphic and isohumic; f)
 147 Calcareous brown soils from thin residual terraces ; g) Gleyic soils from clayey alluvium of streams and marly lowlands.

148

149 **2-Materials and Methods**

150 ***Coring and litho-stratigraphic analysis***

151 Three cores were retrieved from the basin in December 2014 using a Geotool GTR 790 corer with a
 152 diameter of 7 cm. Drilling areas were selected after a preliminary survey consisting of c. 30 hand
 153 auger litho-stratigraphic logs distributed along several cross-sections (Mayoral et al., 2018). NAR2
 154 (depth 230 cm) was situated in the lower part of the depression, whereas NAR3 (depth 227 cm) and
 155 NAR4 (depth 284 cm) were located in a drier peripheral area (Fig. 1C and 2). NAR4 was not subject to
 156 multi-proxy palaeoenvironmental analysis and is therefore not presented in this work. Detailed litho-
 157 stratigraphic and sedimentary description of NAR2 and NAR3 cores was performed (See Table 1 and
 158 Fig. 3), in order to refine the description of sedimentary units (SU) from previous work (Mayoral et
 159 al., 2018).

160 Figure 2. Selected stratigraphic cross-sections of the basin (P1 and P2, adapted from Mayoral et al., 2018) with location of
 161 cores NAR2 and NAR3 (see also Fig. 1C).

162

163 ***Radiocarbon dating and age-depth modeling***

164 Radiocarbon database from the first study (Mayoral et al., 2018) was completed with 9 AMS
 165 radiocarbon dates in cores NAR2 and 3 (see Table 2). Two were performed in selected gastropod
 166 shells (*Vallonia pulchella*) in order to test if terrestrial species could locally provide accurate
 167 radiocarbon ages in the absence of other datable material. Other dates were performed on
 168 microcharcoal manually concentrated using a binocular microscope, after deflocculating sediment
 169 with sodium hexametaphosphate and sieving at 500 and 100 µm. Raw radiocarbon dates were
 170 calibrated with Calib 7.0 (Stuiver and Reimer, 1993) and IntCal13 calibration curve (Reimer et al.,

2013). Age-depth models (ADM) were built using smooth spline method under CLAM (Blaauw, 2010), based on radiocarbon data and unambiguous stratigraphic correlations between cores (Fig. 3). Sediment Accumulation Rate (SAR) was then calculated.

Micromorphological analysis

A half-section of NAR2 core was cut between 64 and 195 cm in 11 micromorphological blocks (see Fig. 3). After induration, thin sections were made from these blocks at the OMEAA laboratory of UMR 5600 EVS (University Lyon 2) following a common protocol (Guilloré, 1980). Thin section description was performed using a Leica M80 binocular microscope (x2.5 to x60) and a Leica DMLP polarizing microscope (x16 to x400), under Cross-Polarized Light (XPL) and Plane Polarized Light (PPL), and according to state-of-the-art references (Delvigne, 1998; Loaiza et al., 2015; MacKenzie et al., 1982; Scholle and Ulmer-scholle, 2003; Stoops, 2003). A Leica camera was used to take microphotographs and measurements. Micromorphological features were semi-quantitatively recorded (see Fig. 4 to 6 and Table 3 in Supplementary Information (SI)) and interpreted on the basis of up-to-date reference works (Macphail and Goldberg, 2018; Nicosia and Stoops, 2017; Stoops et al. 2010b). Micro-charcoal was semi-automatically quantified using image analysis software (Aphelion Dev) and microphotographs taken each centimeter under Oblique Incident Light (OIL) (Berger et al., 2016). Reddish scoria particles, whose local sources are limited to the Puy de Corent slopes in the eastern part of La Narse catchment (Bouiller, 1979), were manually counted and their surface measured each centimeter with a binocular microscope in order to be used as a tracer of sedimentary sources.

X-Ray Fluorescence

X-Ray Fluorescence (XRF) measurements were performed in NAR2 and NAR3 cores using an Avaatech XRF core-scanner (EDYTEM, Université Savoie Mont Blanc). Cores were analyzed with 5 mm resolution under 10 kV (1mA, 10s) and 30 kV (0.75 mA, 30s) beams generated by a Rhodium anode. Results include detection in counts per second (cps) for Al, Si, P, S, Cl, K, Ca, Ti, Cr, Mn, Fe, Rh, Cu, Zn, Ga, Br, Rb, Sr, Y, Zr, Nb, Mo, Pb and Bi. A Principal Component Analysis (PCA) was performed using

Xlstat software on selected elements of NAR2 (Fig. 8), in order to assess relationships between elements and with sedimentary units (Bajard et al., 2016; Birks & Birks, 2006 ; Sabatier et al., 2010). To improve the PCA interpretation and especially to refine the sedimentary source identification, we added 20 supplementary individuals (not contributing to the PCA) obtained from XRF analysis of a core situated in the top of the Puy de Corent (Fig. 1C). These individuals reflect the geochemical signature of a 100% volcanic soil and sediment (data from Mayoral, 2018). Elementary ratios were selected as palaeoenvironmental proxies based on PCA analysis, local geology and soils, litho-stratigraphy, micromorphological analysis and sedimentological data, and following up-to-date references (e.g. Croudace and Rothwell, 2015).

Sedimentological analysis

Grain-size analysis was undertaken on NAR2 core using a Coulter LS230 granulometer. We analyzed contiguous 2cm-thick sediment slices of NAR2, between 30 and 230 cm (see Fig. 3). Data were then processed under Gradistat (Blott and Pye, 2001), and resulting statistical parameters (D50 and D99) were used to build a Passega (or CM) diagram (see Fig. 8) in order to identify hydro-sedimentary processes (Bravard and Peiry, 1999; Passega, 1977).

Magnetic susceptibility (MS) of NAR2 and NAR3 was measured using a Bartington MS2E meter. Four measurements were performed each cm, and the mean value was retained in order to integrate signal variability (Dearing, 1999). Loss on ignition (LOI) was used to assess contents in organic matter (OM) and carbonates in both cores. We analyzed contiguous 2cm-thick sediment slices (see Fig. 3) of NAR2 (30-230 cm) and NAR3 (54-227 cm), following a standard two-step protocol (Heiri et al., 2001).

Malacological analysis

Malacological analysis was performed in both cores in order to assess the development of the structure of the vegetation cover and to reconstruct hydrological dynamics in the depression. We sampled contiguous 2cm-thick sediment slices (see Fig. 3) in NAR2 (70-202 cm, half-section) and NAR3 (84-201 cm, full section). Samples were sieved at 500 µm and studied under binocular microscope.

1
2
3 221 When necessary, samples from the same SU were grouped in bigger sets (4 to 14 cm, see Tables 4
4
5 222 and 5 in SI) in order to reach a significant number of shells, since at least 150 individuals per sample
6
7 223 were required to run a reliable statistical analysis (Evans, 1972). Samples comprising a boundary
8
9 224 between two SU were not analyzed. Determination of species was performed on the basis of
10
11 225 identification guides (Horsák et al., 2013; Kerney & Cameron 2006; Welter-Schultes, 2012). 23
12
13 226 terrestrial and 14 freshwater species have been listed (Tables 4 and 5 in SI). On the basis of the
14
15 227 faunal lists, an analysis of the species composition of the malacological assemblage of each sample
16
17 228 was carried out and each species was assigned to an ecological group, which was defined in the light
18
19 229 of the habitats described in the species guides used for determination. Terrestrial species were
20
21 230 divided into four ecological groups (shade-demanding species, mesophile species, marshland species
22
23 231 and open-ground species) while freshwater species were combined in a single group (Fig. 9).
24
25
26
27
28
29

30 **232 3-Results**

31
32
33 233 **3.1 Stratigraphy and age-depth models**

34
35 234 Litho-stratigraphy of both cores is broadly similar, with some thickness and grain-size variability due
36
37 235 to lateral change of facies and position in the depression (see Figs. 1 to 3). Four Sedimentary Units
38
39 236 (SU) are concerned by multi-proxy analysis: SUIII.2-3, SUIII.1b, SUIII.1a and SUII.3. For a complete
40
41 237 description of NAR2 and NAR3 litho-stratigraphy, see Table 1. SU III.2-3 consists of grey silty clays,
42
43 238 including (in the core NAR2) two well-sorted and fining-upwards coarse sand levels. SUIII.1.b is
44
45 239 composed of more or less dark grey silty clay with traces of pedogenesis: this layer is representative
46
47 240 of the locally extended hydromorphic and isohumic soils, so-called Limagne “dark earths” (Bornand
48
49 241 et al., 1968). SUIII.1a is similar to SUIII.1b, but has a more brownish color and includes several
50
51 242 oxidation mottles, indicating drier or more fluctuating hydrological conditions. Finally SUII.3 is
52
53 243 composed of black and very dark grey silty clays, rich in non-degraded vegetal debris, suggesting
54
55 244 deposit under palustrine conditions (Mayoral et al., 2018).
56
57
58
59
60

245 Table 1. Litho-stratigraphic description of cores NAR2 and NAR3, and stratigraphic correlations between them.

NAR2		SU	NAR3		
Description (Munsell color, grain size, inclusions, pedofeatures)	Cm.		Cm.	Description (Munsell color, grain size, inclusions, pedofeatures)	
2,5Y4/2 Silty clay with macrocharcoal and OM remains, few fine sands, bioturbation (current topsoil)	0-12	I	0-25	2,5Y3,5/2 Silty clays with darker mottles. Some fine to medium sparse sands. Organic remains and malacoremain. Bioturbation (current topsoil)	
2,5Y4/2 Silty clay to clayey silt, abundant OM remains, few fine sands, bioturbation (roots)	12-16				
2,5Y4/2 Silty clay, some fine sands, few small charcoal, rootlets	16-26				
2,5Y4/2 Clayey silt, pale yellow inclusions (diatomite), small yellowish brown oxidation mottles, small charcoal, some fine to medium sands, rare malacoremain	26-35	II.1	-	-	
2,5Y4,5/2 Clayey silt, rare sands, abundant pale yellow inclusions (diatomite), few small yellowish brown oxidation mottles, some malacoremain	35-44				
2,5Y5/2 Silty clay, darker dots, some malacoremain	44-59				
2,5Y5/2 Silty clay, sparse fine to medium sands, darker inclusions from underlying unit, irregular inferior limit, abundant malacoremain	59-64	II.2	25-47	2,5Y3,5/2 Silty clays, some sparse medium sands	
5Y4/1 Silty clay, sparse fine sands, darker inclusions from underlying unit, incipient subangular to granular aggregation, abundant malacoremain	64-70	II.3	47-54	5Y3/2 Silty clays, darker inclusion from underlying unit, and brown from overlying unit. Rare medium sands, rare malacoremain	
2,5Y2/0 Silty clay, brown inclusions from underlying unit, few fine sands, small organic debris and abundant OM, incipient granular to crumbly aggregation, abundant malacoremain.	70-79		54-61	5Y2,5/1 Silty clays, with darker mottles. Abundant malacoremain and sparse fine to medium sands.	
5Y4/1 Silty clay, several black inclusions from overlying unit, several small yellowish brown oxidation mottles, few malacoremain.	79-85	III.1a	61-76	5Y3,5/2 Silty clays, brown oxidation mottles (top), some darker mottles from overlying unit. Rare fine to medium sands.	
5Y4/1 Silty clay, rare black inclusions from overlying units, rare oxidation mottles, rare malacoremain	85-90				
5Y4/1 Silty clay, rare fine sands, rare malacoremain	90-100		76-103	5Y4/1,5 Silty clays, small malacoremain	
5Y4/1 Silty clay, incipient granular aggregation to the base, few malacoremain	100-114	III.1b	103-113	5Y3/1 Silty clays, small malacoremain.	
5Y3,5/1 Silty clay, incipient crumbly aggregation, several malacoremain,	114-122		113-128	5Y3/2 Silty clays, small malacoremain	
5Y3/1 Silty clay, incipient crumbly aggregation, abundant malacoremain	122-132		128-147	5Y3/2 Silty clays, small malacoremain	
5Y3/1 Silty clay, incipient crumbly aggregation (top), abundant malacoremain	132-154	III.2-3	147-158	5Y3/2 Silty clays, several malacoremain	
5Y4/1 Silty clay, sparse fine sands, abundant darker mottles from overlying unit	154-158		158-172	5Y3/1,5 Silty clays, small malacoremain	
5Y4/1 Slightly silty clay, few dark mottles, one dark lamination, some sparse fine sands	158-163				
5Y4/1,5 Silty clays, several fine to medium sands, several small oxidation mottles, irregular contact with underlying unit. One dark lamination.	163-168/171				
5Y4/1,5 Fine to coarse sands, poorly rounded grains (limestone, basalt, quartz). Fining upwards sorting. Few silts and clays. Irregular top and base.	168/171-178/180				
5Y4/1 Silty clays abundant sparse fine to coarse sands (limestone, basalt, quartz), rare malacoremain.	178/180-185				
5Y4/1,5 Fine to coarse sands (limestone, basalt, quartz), poorly rounded, silts and clays. Fining upwards sorting (poorly marked). One angular basaltic gravel at the base.	185-194		172-193	5Y2,5/1 Silty clays, small malacoremain,	
5Y4,5/1 Silty clay, some sparse fine sands	194-196				
5Y4,5/1 Silty clay, with intercalations of 5Y6/2 heavy clay, including oxidation mottles. Sparse fine to coarse sands	196-202		IV.1b	193-203	5Y5/1 (top) to 7/2 (base, with several darker intercalations) Heavy clays.
5Y6/2 Heavy clay with oxidation mottles and darker mottles from upper units (bioturbation?). Rare and sparse fine sands	202-212/214				
5Y6/2 Slightly silty clay with oxidation mottles, some fine to medium sands	212/214-217				
5Y6/2 Heavy clay with rare oxidation mottles, rare fine to medium sands	217-222				
5Y6/2 Slightly silty clay, big oxidation mottles, sparse fine to medium sands	222-228				
5Y6/2 Heavy clay, rare oxidation mottles, sparse fine to medium sands	228-230				
		V	203-220	5Y6/2 Heavy clays. Rare and sparse fine sands. 2 dark laminations. Oxidation mottles.	
			220-225	5Y6/2,5 Heavy clays. Rare and sparse fine to coarse sands. Very abundant oxidation mottles. One dark lamination (base).	
			225-227	5Y6/2,5 Heavy clays, Rare and sparse fine to coarse sands. Few oxidation mottles.	

246 The radiocarbon database includes 14 dates distributed within the two cores and performed mainly

247 on charcoal (Table 2). The two dates on gastropod shells were rejected because they provided

248 significantly older results than charcoal, clearly inconsistent with the chrono-stratigraphic

249 framework. The Age-Depth Model (ADM) constructed for NAR2 (smooth spline) was extrapolated to

1
2
3 250 230 cm and SAR was calculated, showing a peak c. 2200-2300 cal BP (Fig. 3). Using radiocarbon and
4
5 251 stratigraphic correlations with NAR2 (SUIV.1b and SUII.3), a less robust (especially under 150 cm) but
6
7 252 nevertheless satisfactory ADM was also constructed for NAR3. SAR in NAR3 shows a disproportionate
8
9 253 peak, between two comparable dates (Table 2), suggesting a virtually instantaneous deposit such as
10
11 254 flood overbank deposits or anthropogenic backfill linked to nearby Roman archaeological remains
12
13 255 (Fig. 1 and 2). The best age-model estimation from both models was used to discuss multi-proxy
14
15 256 analysis results.
16
17
18

19 257 Figure 3. Litho-stratigraphy, stratigraphic correlations, sampling and age-depth model of NAR2 (left) and NAR3 (right) cores.
20
21
22 258
23
24 259
25
26 260
27 261
28
29 262
30
31 263
32
33 264
34 265
35
36 266
37
38 267
39
40 268
41 269
42
43 270
44
45 271
46
47 272
48
49 273
50 274
51
52 275
53
54 276
55
56 277
57 278
58
59 279
60

Table 2. Radiocarbon dates from NAR2 and NAR3 cores. 1,3,4,5 and 9 were published in Mayoral et al. (2018). *Dates in italic were rejected.*

Nº	Core	Depth (cm)	Lab Code	Material	¹⁴ C yr. BP	Cal BP (median, 2σ)	Cal BC/AD (median, 2σ)
1	NAR2	38-40	Poz-86197	Microcharcoal	485 ± 30 BP	522 ± 21	1428 ± 21 cal AD
2	NAR2	70-72	Poz-71623	Microcharcoal	1505 ± 30 BP	1418 ± 100	532 ± 100 cal AD
3	NAR2	76-78	Poz-86198	Microcharcoal	1540 ± 40 BP	1439 ± 89	511 ± 89 cal AD
4	NAR2	106-108	Poz-71624	Microcharcoal	2035 ± 35 BP	2006 ± 106	56 ± 106 cal BC
5	NAR2	142-144	Poz-71625	Microcharcoal	2410 ± 40 BP	2524 ± 176	574 ± 176 cal BC
6	NAR2	160-162	Beta-434189	Microcharcoal	2460 ± 30 BP	2537 ± 171	587 ± 171 cal BC
7	NAR2	183-184	Poz-86199	Microcharcoal	3415 ± 30 BP	3699 ± 120	1749 ± 120 cal BC
8	NAR2	190-192	Poz-86200	Microcharcoal	3910 ± 30 BP	4335 ± 86	2385 ± 86 cal BC
9	NAR2	196-200	Poz-86201	Microcharcoal	4280 ± 60 BP	4831 ± 206	2881 ± 206 cal BC
10	NAR3	98-100	Poz-86203	Microcharcoal	1540 ± 50 BP	1437 ± 102	513 ± 102 cal AD
11	NAR 3	114-120	Poz-103585	<i>Vallonia pulchella shells</i>	2425 ± 30 BP	2526 ± 172	576 ± 172 cal BC
12	NAR3	120-122	Poz-86204	Microcharcoal	1930 ± 35 BP	1901 ± 88	49 ± 88 cal AD
13	NAR3	130-132	Poz-86205	Microcharcoal	2010 ± 30 BP	1963 ± 78	13 ± 78 cal BC
14	NAR 3	174-181	Poz-103586	<i>Vallonia pulchella shells</i>	6480 ± 50 BP	7379 ± 98	5429 ± 98 cal BC

3.2 Micromorphology

Detailed micromorphological descriptions can be found in Table 3 in SI. The key features used to define micromorphological units (named MI to MVII) were semi-quantitatively recorded in Fig. 6.

Units MVII and MV (195-188 and 178-166 cm) are formed by roughly sorted coarse to fine alluvial sand with fining-upwards sorting. Sand is rich in carbonated and volcanic grains (basalt with analcime crystals and scoria, see Fig. 4), and rounded fragments of tuffaceous/pisolithic coatings and biospheroids. These fragments together with some organic remains (chiefly vegetal tissues, bone or charcoal) and inherited pedosedimentary aggregates, indicate a polyphased genesis of these sandy

291 layers. Both are likely the result of an intense hydro-sedimentary event that eroded soils and
 292 riverbed deposits of the catchment, separated by a phase of incipient soil formation (MVI).

293
 294
 295
 296
 297
 298
 299
 300
 301
 302
 303
 304
 Figure 4. Selected micromorphological features of lower NAR2 (Micromorphological Units MVII to MIV, see text and Fig. 6). A) Cluster of mite droppings, microcharcoal-rich micromass (MIV, N211, PPL-Plane Polarized Light). B) Platy microstructure (MIV, N211, transmitted light). C) Spore remains (MIV, N211, PPL). D) Rounded pedosedimentary aggregate (reddish matrix), surrounded mainly by carbonated micritic sands (MV, N212B, XPL-Crossed Polarized Light). E) Bone fragment (MVI, N213, XPL). F) Fragment of micritic to micro-sparitic carbonated root concretion (MIV, N212A, XPL). G) Contact (arrows) of coarse sands with silty clays. Note the big stromatolitic/tuffaceous fragment of limestone, with a secondary microlaminated calcite coating (MV, N212B, XPL). H) Fragment of basalt with a coating of microlaminated calcite (micrite and microsparite) and rounded by transport (MVI, N213, XPL). I) Volcanic reddish scoria fragment, including translucent plagioclases (MV, N212B, OIL-Oblique Incident Light). J) Cluster of charcoal and in-situ charred remains (MIV, N211, PPL). K) Portion of dark matrix, with more abundant coarse fraction, more humic and enriched in microcharcoal, probably from a surficial soil horizon (MIV, base of N211, OIL). L) Clayey aggregates with striated B-Fabric (arrows), likely degraded fragments of slaking crust (MIV, N212A, XPL).

305 Sediment forming MVI unit (186-178 cm) has finer texture, with abundant clayey matrix.
 306 Pedofeatures suggest some soil development despite a poorly developed microstructure, with few
 307 orthic sparite nodules and organo-manganic aggregates, within abundant floated materials (bone
 308 and charcoal).

309 Unit MIV (172-152 cm) matrix is made of silty clays with few coarse particles, and
 310 micromorphological features (microstructure, pedofeatures) broadly indicate more mature soil
 311 development than in previous phases. Reduced porosity, few biospheroids and presence of calcite
 312 and manganese nodules suggest a massive soil, with fluctuating water table level and short but
 313 repeated water saturations of soil (Courty et al. 1989; Durand et al., 2010; Freytet and Verrecchia,
 314 1998; Lindbo et al. 2010; Zamanian et al., 2016). Abundance of mite droppings (Fig. 4 and 6) instead
 315 of traces of earthworm activity indicate massive soil development under damp conditions, which
 316 would be consistent with the reconstruction of a wet grassland environment (Gerasimova and
 317 Lebedeva-Verba, 2010 ; Jeffery et al., 2010 ; Kooistra and Pulleman, 2010).

318 The top of the unit presents striking micromorphological differences with the underlying units, such
 319 as platy microstructure, increased porosity (vughs, small rootlets channels), calcitic earthworm

320 biospheroids and more abundant organic remains including micro- and macrocharcoal (Fig. 4 and 6).

321 In addition, some small aggregates with striated b-fabric are likely fragments of a slaking crust from

322 superficial soil palaeohorizons (Fig. 4). Taken together, these features clearly indicate a major soil

323 disturbance at the summit of unit MIV that might result from agricultural activities and use of fire to

324 clear the ground (Adderley et al., 2010; Deák et al., 2017a; Jongerius, 1970; Macphail et al., 1990;

325 Pagliai and Stoops, 2010a; Spek et al., 2003).

326 MIII unit (148-100 cm) shows confirmation of the new soil dynamics already outlined at the top of

327 MIV, namely agricultural activities probably involving use of fire. MIII has a silty clay matrix with rare

328 coarse grains, and well-developed blocky subangular to granular microstructure (Fig. 6). Intrapedal

329 porosity is dominated by small grass channels. The lack of intra-aggregate biogenic macro-porosity

330 despite abundant organic matter (OM) and biospheroids, and lack of true granular or excremental

331 microstructures, strongly supports human-induced reaggregation by repeated ploughings (Adderley

332 et al., 2010; Macphail et al., 1990 ; Spek et al., 2003). Absence of coarse textural features such as

333 silty-clay coatings is not critical here, since they are not a *sine qua non* condition for cultivated

334 horizons (Deák et al., 2017a; Usai, 2001), especially in fine-textured carbonated rocks context: in

335 these cases, alternative indicators are charcoal increase, loss in gastropod diversity (Macphail and

336 Goldberg, 2018; Whittle et al., 1993) and/or loss of micro-arthropods population due to soil

337 disturbance (Jeffery et al., 2010).

338 Vegetal debris, fine organic matter and biospheroids, and especially microcharcoal are clearly more

339 abundant than observed before and are distributed homogeneously within the unit (Fig. 6). These

340 features indicate the continuous development of a relatively homogeneous organo-mineral A

341 horizon (Adderley et al., 2010; Durand et al. 2010; Gerasimova and Lebedeva-Verba, 2010; Stoops et

342 al., 2010a). Resulting soil profile could be described as isohumic with cumulic and slightly

343 hydromorphic processes.

344 Redox pedofeatures of MIII are of limited intensity and vertically heterogeneous, indicating that they
345 corresponded to repeated flooding of the depression with variable frequency and duration (Kovda
346 and Mermut, 2010 ; Lindbo et al., 2010). Together with other pedofeatures (erosion markers,
347 carbonates, microstructure) these redox indicators allowed us to distinguish four alternating sub-
348 phases within MIII (see Fig. 6). Micromorphological indicators (microstructure, calcite and iron
349 nodules, iron hypocoatings, spores, see Fig. 4) suggest that MIII.4 and MIII.2 were affected by more
350 intense watertable fluctuations with repeated and long-term floods, alternating with dry phases
351 (Fedoroff and Courty, 2002; Kovda and Mermut, 2010; Lindbo et al., 2010; Stoops et al., 2010a).
352 Hydrological conditions were probably drier and more stable for phases MIII.3 and MIII.1, less
353 affected by seasonal floodings (few calcite and iron nodules). Additionally, micromorphological
354 evidence (macrocharcoal, pedosedimentary aggregates) indicates increased soil erosion and fires
355 during MIII.3 (Adderley et al., 2010 ; Fedoroff et al. 2010).

356 MII unit (100-79 cm) is broadly comparable to MIII. Increasing soil erosion in the catchment is
357 suggested by more abundant volcanic mineral fraction and well-rounded calcite biospheroids. More
358 abundant organic matter features (especially macrocharcoal) and presence of some incipient
359 microlaminated clay coatings (partly oriented, limpid to dusty) in underlying unit (MIII) point to
360 increasing soil disturbance and illuviation, probably connected to more intensive agricultural activity
361 (Kühn et al., 2010) in a context of general low accretion and soil profile stability. Atypical redox
362 features distribution (iron hypocoatings at the top, and manganic nodules at the base) together with
363 other micromorphological features, suggest a broadly drier phase. This was subsequently followed by
364 very wet conditions probably due to floods during MI deposition (see below), similarly to paddy soil
365 redox patterns (Stolt and Lindbo, 2010).

366

367

368

369

370

371

372

373

374

375

376

377

378

379

380

381

Figure 5. Selected micromorphological features from upper NAR2 (Micromorphological Units MIII to MI, see text and Fig.6). A) Orthic tuffaceous concretion, from aggregation of smaller micritic elements and pseudomorphs (MI, N204, XPL-Crossed Polarized Light). B) Tuffaceous calcite capping. Note dark micromass, rich in organic matter (MI, N204, XPL). C) Orthic calcite nodule in a dark cristallitic to isotropic micromass (MI, N204, XPL). D) Micromass rich in calcitic grains strongly bioturbated and reorganized by biological activity (MI, N204, XPL). E) Complex microstructure, subangular with granular substructure or crumbly subangular (MI, N204, transmitted light). F) Diatoms embedded in carbonate-rich micromass (MI, N204, PPL-Plane Polarized Light). G) *Characeae* oogon. Note the two different types of micromass: brown, clayey, rich in organic fragments and microcharcoal (base) vs. massive micritic-microsparitic micromass (top) (MI, N204, XPL). H) Iron and micritic hypocoatings around a chamber and fissural to canalicular voids (MIII, N208, XPL). I) Subangular blocky microstructure of an organo-mineral unit (MIII, N207, transmitted light). J) Iron hypocoating and biospheroid, note silty clay micromass rich in microcharcoal and small organic fragments (MII, N205, PPL). K) Granular microstructure of a organo-mineral unit, note partial collapse of porosity due to secondary clogging (MIII, N210, transmitted light). L) Silty clay matrix highly impregnated by oxidized iron, and injection of matrix aggregates (rich in organic matter) from upper layers (MII, N205, XPL). M) Concentration of micritic to microsparitic calcite in the matrix (and in voids), some evolving to nodules (MIII, N208, XPL). N) Calcite nodule (micritic to microsparitic) in development by impregnation of the matrix (MIII, N209, XPL). O) Small bone fragment embedded in a silty clay matrix with microcharcoal and organic microdebris (MII, N205, PPL).

382

383

384

385

386

387

388

389

390

391

392

393

394

395

396

MI (79-64 cm) presents micromorphological features radically different from all other units. The matrix is globally very cristallitic, extremely rich in brown to black organic fragments with frequent microsparitic to sparitic calcite nodules (orthic), and abundant bio-mineral microfossils (ostracods, *characeae* pseudomorphs and oogons and tuffaceous concretions, see Fig. 5 and 6) indicating aquatic conditions (Nicosia and Stoops, 2017; Scholle and Ulmer-scholle, 2003). This unit can globally be interpreted as an aquatic environment with marked palustrine features. Very abundant and rounded micro- and macrocharcoal fragments suggest fires and erosion on the slopes of the catchment.

389

390

391

392

393

394

395

396

Detailed micromorphological analysis enabled us to discern a threefold structure within MI unit (Fig. 6). MI.3 is characterized by abrupt development of palustrine conditions (very abundant organic matter) above the MII relatively dry palaeosoil. These new conditions are more probably the result of drainage deterioration and strong and permanent flooding than of a rise of groundwater-level (see unit MII features). Peak of macro- and microcharcoal (Fig. 6) and inclusion of soil aggregates from MII indicate strong and local soil erosion during this process. Water level rose during phase MI.2 and conditions became lacustrine (disappearance of pedogenic features), with strong authigenic carbonates production (abundant calcite nodules and tuffaceous concretions, and sometimes

1
2
3 397 diatoms, see Fig. 5). Finally water level decreased slightly in MI.1, as suggested by reoccurrence of
4
5 398 channels and biospheroids, more organic micromass with charcoal, and less calcite nodules and
6
7 399 tuffaceous concretions. However, posteriority of these “drier” pedofeatures due to later phases of
8
9
10 400 total emersion and erosion (not analyzed here) cannot be excluded.
11
12
13 401
14
15
16
17
18
19
20
21
22
23
24
25
26
27
28
29
30
31
32
33
34
35
36
37
38
39
40
41
42
43
44
45
46
47
48
49
50
51
52
53
54
55
56
57
58
59
60

Accepted Manuscript

Figure 6. Summary diagram of main micromorphological features of NAR2 between 65 and 195 cm. Bars width indicates their relative abundance (rare, few, several /some, abundant, very abundant, see Table 3 in Supplementary Information), or alternatively their development degree. Scoria and microcharcoal are quantified using image analysis (IA). C/F: Coarse/Fine ratio, here 20 μ m.

Accepted Manuscript

3.3 Geochemistry and sedimentology

The Sedimentary Units (SU) are well differentiated on the Passega (or CM) diagram of NAR2 (Fig. 8B). Most samples are poorly sorted (i.e. far from C=M line) due to common coarse particles embedded in abundant fine matrix. This is certainly due to long-term pedoturbation of most part of this low-aggradation pedo-sedimentary sequence, making it difficult to understand “pure” sedimentary processes. SUII.1, II.2-3 and II.3 probably refer to very low energy sedimentary processes (decantation phase) mixed with relatively rare and weak detrital inputs (graded to uniform suspension), likely formed under aquatic conditions. At the opposite, SUIII (III.1a, 1b and 2-3) has a CM signature implying varied processes of transport and deposition (decantation, graded suspension and rolling). Excepting sandy layers, deposits have a broadly fine but highly variable grain-size, which is consistent with a low-energy alluvial-palustrine plain with reduced aggradation, implying permanent pedoturbation and homogenization of flood deposits.

The XRF elementary signals obtained for NAR2 and 3 are globally consistent with main stratigraphic changes and with sedimentological indicators (Fig. 7A and B). Magnetic Susceptibility (MS) and D50 are interrelated and correlated with Fe, Si and Ti (except in sandy layers of NAR2), and with Fe, Zr and Rb in NAR3. Organic matter (OM) content is inversely correlated to carbonate content in both cores (see Fig. 7). Variables are well differentiated in the PCA on selected elementary signals of NAR2 (Fig. 8A), where the first 2 components count for 78.6% of the variability. The main axis (64.9%) represents the opposition between allochthonous detrital inputs (positive scores, terrigenous elements) and authigenic elements production under wet or aquatic conditions (negative scores, mainly Ca and Sr carbonates and Mn). The second axis represents the balance between siliciclastic materials (positive scores: Si, Al) and volcanic materials (negative scores: Zr, Ti). SUs are well differentiated in the distribution plot following main axes of the PCA (Fig. 8A). SUI to SUIII show mainly volcanic sediment influence, SUIII being the more detrital unit in the sequence (excepting sands). The gradual shift from SUIII to SUII.1 (from positive towards negative values of main axis) strongly suggests drainage degradation and installation of aquatic conditions.

431 Five endmembers could therefore be identified depending on their geological sources and authigenic
432 or allochthonous origins. A first one includes Zr and Ti, which are especially abundant in volcanic
433 rocks (Mielke, 1979 ; Salminen et al., 2005) and likely come from volcanic materials of surrounding
434 reliefs. The position of 20 supplementary individuals (red squares, not contributing to the PCA, see
435 methods) obtained from XRF analysis of a core on volcanic-derived clays (Mayoral, 2018) confirmed
436 this interpretation (Fig. 8A).

437 Si, Al and Pb are more abundant in felsic materials (Mielke, 1979; Wedepohl, 1978) and are therefore
438 suggestive of sedimentary inputs derived from silt-rich marls, very abundant in Limagne lowlands.
439 Finally Fe and Zn, more abundant in volcanic rocks but also present in felsic materials, form together
440 with Rb an intermediate endmember, indicating mixed inputs or a source from a residual terrace of
441 the Allier river, which borders the northern margin of the depression (Fig. 1B and C). Ca and Mn form
442 a typical chalco-manganic endmember related to wet conditions and authigenic carbonate formation
443 (Salminen et al., 2005; Wedepohl, 1978). The last endmember is formed by Sr alone, isolated from Ca
444 and Mn due to its higher abundance in volcanic rocks (Mielke, 1979).

445 Based on these data, on geochemistry of rocks and soils from the study area, and on existing
446 literature, we interpreted the local palaeoenvironmental significance of selected elementary ratios.
447 Zr content is relatively high in coarse sediment as it is related to the presence of detrital heavy
448 minerals (zircon, sphene), and is lower in finer sediment where heavy minerals are scarcer. By
449 contrast Rb is often higher in finer fraction of sediment due to its very strong sorption by clay
450 minerals (Salminen et al., 2005). In NAR2 and NAR3 cores, Zr/Rb ratio appears positively correlated
451 to D50 of the sediment, both in its fine (<50µm) and coarse (>50µm) fractions (see Fig. 12B in
452 Supplementary Information). Consequently we propose to interpret Zr/Rb as a grain-size proxy in our
453 cores.

454 Pb content in European soils and floodplain sediments is related to two main factors: lithology
455 (natural Pb mineralisations) and anthropogenic contamination, i.e. historical mining or industrial

activities (Salminen et al., 2005). Calcareous and volcanic rocks, such as those found in La Narse de la Sauvetat catchment, are not a significant source of lithogenic Pb. Additionally, considering the very small size of the catchment and its uncomplicated geology, lithogenic Pb fluxes can be assumed to be more or less constant in the sedimentary record analyzed in NAR2 and NAR3, and anomalous Pb enrichments are certainly of anthropogenic origin. A simple way to discriminate signal of anthropogenic Pb from the lithogenic Pb background is normalization using a lithogenic and chemically stable trace element (Arnaud et al., 2004, 2006). Therefore we propose to use Pb/Rb as a potential indicator of anthropogenic Pb contamination (and therefore metallurgic activity) in La Narse de la Sauvetat sedimentary record, especially when ratio peaks appear dissociated from detrital inputs proxies.

Fe is in general terms much more abundant in volcanic than in sedimentary rocks (Salminen et al., 2005), and consequently also in soils developed in volcanic materials (Legrand et al., 2007). Geochemical studies in the Sarliève palaeolake catchment, also situated in southern Limagne and largely sharing lithology and superficial formations with La Narse de la Sauvetat catchment (Bornand et al., 1968; Bouiller, 1979; BRGM, 1973), show that local volcanic soils and rocks were Fe-enriched, and clearly distinguishable from Ca-enriched soils developed on Limagne calcareous bedrock (Fourmont et al., 2009). Within La Narse catchment, soils and fine sediment from the top of the Puy de Corent (*i.e.* exclusively derived from volcanic rocks. See Fig. 1), show much lower values of Ca and higher values of Fe (and hence significantly higher Fe/Ca ratio) than samples from NAR2 and NAR3, situated in calcareous lowlands (see Fig. 12A in Supplementary Information -data from Mayoral, 2018-). Then, we propose to use Fe/Ca to trace fine detrital inputs derived from erosion of surrounding volcanic soils and surficial formations into La Narse Basin.

478

Figure 7. A) Selected elements and sedimentological data for NAR2. Values are in 10^{-5} SI (Magnetic Susceptibility-MS-) and in counts per second (CPS) for the XRF. B) Selected elements and sedimentological data for NAR3.

Figure 8. A) PCA biplot of selected geochemical variables according to dimensions 1 and 2, individuals are distributed by Sedimentary Unit. Note supplementary individuals (red squares, data from Mayoral et al., 2018). B) Passega or C-M diagram of NAR2 with grain-size data by Sedimentary Unit. Grey area represents reference C-M diagram by Passega (1977).

3.4 Malacology

Seven environmental phases were reconstructed in NAR2 (phases 2A to 2G in Fig. 9). In phase 2A (202-194 cm) freshwater species count 50% of the total number of individuals. In the terrestrial fauna, shade-demanding molluscs are scarce (Fig. 9A). In phase 2B (194-170 cm) freshwater species decrease to 30% while proportions of shade-demanding species increase. Whether this ecological group shows its highest proportions of the whole core, the species from this group are not restricted today to forest environments and may have lived in tall grass patches in Limagne plain. The proportions of freshwater species increase in phase 2C (170-158 cm) and despite a small number of shells, strong differences are highlighted in the ecological composition of the molluscan assemblage attributed to this phase with decreasing proportions of shade-demanding species (Fig. 9A). The 2D phase (158-142 cm) is characterized by a strong dominance of open-ground species, which represent 60% of the total number of individuals. *Vallonia pulchella*, which lives today in wet grassland environments, is the most abundant species (Table 4 in Supplementary Information-SI). In addition, freshwater species represent only 20% of the assemblages (Fig. 9A). *Galba truncatula* is the main species within this group (Table 4 in SI). Its ability to survive dry episodes (Horsák et al., 2013) suggests a phase of contraction of the body of water in the depression and its replacement by wet grasslands. During the phase 2E (142-100 cm), freshwater species increase up to 60% (Fig. 9A). *Galba truncatula* and *Anisus leucostoma* dominance suggest seasonal incursions of water in the sampled locus (Welter-Schultes, 2012). In the terrestrial molluscan fauna, *Vallonia pulchella* is still the dominant species, and this taxon from wet grassland is supported by a diverse set of marshland species (Table 4 in SI). The phase 2F (100-80 cm) is characterized by a dramatic decrease in freshwater species proportions (Fig. 9A). The freshwater species that are able to survive short-term dry episodes sharply decrease in abundance (Table 4 in SI), which indicates a long-lasting depletion of

the water body in the depression. In the terrestrial molluscan fauna, this environmental development is discernible in the decreasing proportions of marshland species (Fig. 9A) and in the replacement of the wet grassland species *Vallonia pulchella* by *Vallonia excentrica* (Table 4 in SI), characteristic of drier open-ground habitats (Welter-Schultes, 2012). Finally, the phase 2G (78-70 cm) is strongly dominated (more than 70%) by a diverse set of freshwater species (Fig. 9A). The main species of this group is *Gyraulus crista* (Table 4 in SI), which is characteristic of permanent and calm small water bodies with rich vegetation (Welter-Schultes, 2012).

In the core NAR3, the full core was dedicated to malacological analysis. As a result, the volume of analyzed sediment was more important, which resulted in more abundant assemblages than in the core NAR2. However, as the volume of sediment analyzed was limited due to the core sampling method, some samples had to be merged to ensure a sufficient number of individuals to carry out a statistical analysis. Five environmental phases were reconstructed (3A to 3E). The phase 3A (201-181 cm) is dominated by species of open-ground habitats, mostly by *Vallonia pulchella* (Fig. 9B). In the phase 3B (181-140 cm), *V. pulchella* is still the main species but the proportions of species living in marshland habitats increase, which indicates wetter environmental conditions. During the phase 3C (140-114 cm), marshland species show decreasing proportions while percentages of species of open-ground environment increase (Fig. 9B). Whether *V. pulchella* remains the most common species within this group, the development of *V. excentrica* reflects the presence of a distinctly drier open-ground habitat. In phase 3D (112-104 cm), freshwater malacofauna significantly increase up to 40% of the total (Fig. 9B). The dominance of *G. truncatula* within this group suggests a seasonally stagnant water body with a damp grassland developed in the margin according to the terrestrial fauna composition. Finally, phase 3E (103-84 cm) is characterized by a sharp increase in freshwater species up to 80-90% (Fig. 9B). The dominance of *G. crista* within this group (Table 5 in SI) reflects a quiet and permanent water flow with rich vegetation.

532

533 Figure 9. Diagrams of specific composition of molluscan assemblages A) NAR2 B) NAR3. Contiguous 2cm-thick sediment
 534 samples were grouped in bigger sets when necessary in order to reach a significant number of shells. Species are
 535 classified by ecological affinities and by order of occurrence.

536

537

538 4-Discussion

539 4.1 Late Neolithic (end of Mid Holocene period)

540 During the Late Neolithic (5000-4150 cal BP, phases N2.1 and N3.1 in Fig. 10, see also Fig. 11), after a
 541 lacustrine phase (see Mayoral et al. 2018), the basin was re-connected to the local drainage system
 542 and developed in a hydromorphic plain (Mn peak at the base of both cores, Fig. 7). Redox conditions
 543 were contrasted: the downstream area (NAR2) was still partly aquatic according to malacological
 544 assemblages, and received detrital inputs from marly slopes of the Puy de Corent (high D50 and
 545 CaCO₃). In the upstream sector (NAR3) higher organic matter (OM) values and malacological data
 546 suggest wet grasslands with more developed soils and oscillating watertable (Fig. 10 and 11). Here
 547 coarser detrital inputs from volcanic soils of the western catchment were predominant (higher MS,
 548 Zr/Rb and Fe/Ca values).

549 Relative openness and diversity of landscapes indicated by malacological assemblages suggest local
 550 transformations by Late Neolithic societies despite these wet conditions in the depression. This
 551 rough picture is consistent with archaeological evidence for this period: findings are very scarce at a
 552 regional level, however they indicate a preference for hillslopes and foothills and a reduced
 553 settlement density in Limagne lowlands during the Late Neolithic, maybe because of drainage
 554 deterioration (Ballut and Argant, 2004; Daugas and Raynal, 1989; Raynal et al., 2003; Trément, 2011).

1
2
3
4
5
6
7
8
9
10
11
12
13
14
15
16
17
18
19
20
21
22
23
24
25
26
27
28
29
30
31
32
33
34
35
36
37
38
39
40
41
42
43
44
45
46
47
48
49
50
51
52
53
54
55
56
57
58
59
60

4.2 Early to Middle Bronze Age

Early and middle Bronze Age (4150-3250 cal BP, phases N2.2-3-4 and N3.2A in Fig. 10, see also Fig. 11) are characterized by a strong increase in hydro-sedimentary activity in the basin. In detail, the period is tripartite: two high-energy alluvial phases (sands) covering the bottom of the basin (see Figs. 2 and 3), separated by a lower energy phase (sandy clays).

The first high-energy deposit was dated at 4464 ± 97 cal BP. It was associated with eroded soils from surrounding volcanic slopes (scoria and nepheline observed in thin section) and from the marly lowlands, but also with erosion of tuffaceous formations from local riverbeds, probably deposited during previous hydro-climatic stability phase. This event was followed by a low-energy hydro-sedimentary phases, dominated by fine volcanic inputs (higher Fe/Ca ratio, Fig. 10) together with an incipient soil development from c. 3850 to 3450 cal BP (weak aggregation and pedofeatures, slightly more organic matter). A second high-energy hydro-sedimentary episode occurred c. 3450 cal BP, also eroding both soils and riverbed formations.

Radiocarbon ages of these two high-energy alluvial phases, similarity with contemporaneous dynamics observed in the Rhone valley (Berger et al., 2007) and consistency with previous studies in Limagne lowlands (Ballut, 2001; Ballut and Guichard, 2005; Trément, 2011; Vital, 2004) indicate that they certainly had a climatic trigger. The first phase was likely associated with the 4.2 kyr. BP climatic event, already documented in eastern and south-eastern French regions (Brisset et al., 2013; Carozza et al., 2015; Magny, 2004). The chronological offset of c. 150-200 yr. (Walker et al., 2019) is likely due to slightly older ages provided by floated charcoal in sandy layers. The second phase was certainly linked to the middle Bronze Age climate event (so-called Löss in the Alpine area), which implied cooler and wetter conditions between 3.5 and 3.2-3.1 kyr. cal BP in western Europe (Berger et al., 2007; Burga et al., 2001; Deák et al., 2017b; Magny et al., 2009). These two high-energy hydro-sedimentary episodes are therefore the first serious sedimentary evidence of 4.2 and 3.5 kyr. BP climate events in Limagne plain, although they have been recently documented in mountainous

highlands of the Massif Central (Chassiot et al., 2018). The intermediary low-energy phase coincided with a more stable hydro-climatic period, detected in alpine lakes and glacial basins (regression phases) and in the Rhone valley by a general trend to pedogenesis and river entrenchment (Berger et al., 2007; Joerin et al., 2006; Magny, 2004; Magny et al., 2009).

NAR3 data show that marginal areas of the basin were also affected by these phases of degraded hydro-sedimentary dynamics: malacological assemblages indicated a progression of marshland environments and biological activity decreased (fall of OM). Data from both cores clearly indicated wetter conditions and absence of significant anthropogenic impact on lowlands soils and vegetation. This situation contrasted with dryer areas of other sectors of Limagne plain where human impact was presumably more significant (Miras et al., 2018). Archaeological findings nevertheless remain rare in Limagne for this period, excepting between 3950 and 3550 BP, when the Limagne was densely occupied by substantial settlements (Couderc, 2019). Taken together, these data suggest a certain degree of adaptation of Early and Middle Bronze age societies to hydro-climatic fluctuations in lowlands. Nevertheless, the potential interaction of these hydro-sedimentary phenomena with anthropogenic impacts on soils during Late Neolithic and Early Bronze Age cannot be clearly assessed from the analyzed pedo-sedimentary record.

4.3 Late Bronze Age and Early Iron Age

The global trend during the Late Bronze Age and first century of the Iron Age (3250-2600 cal BP, phases N2.5A-B and N3.2B in Fig. 10, see Fig. 11) was towards a decrease of hydro-sedimentary activity in the whole basin. Drainage seems slightly degraded with presence of stagnant water especially in central lower areas of the depression (weak OM content, malacological assemblages rich in freshwater species). Soils were then saturated, with a massive structure, limited biological activity

604 and fluctuating watertable. This phase of degraded drainage could partly correspond to the start of a
605 major climate deterioration occurring at c. 2800 BP in western Europe, with cooler and wetter
606 conditions prevailing until c. 2400 BP (Berger et al., 2007; Fletcher, Debret and Sanchez-Goñi, 2013;
607 Holzhauser et al., 2005; Magny et al., 2009; Van Geel and Magny, 2002; Walsh et al., 2019).

608 Despite these unfavorable hydrological conditions in the basin itself, a more open landscape (as
609 indicated by malacology) points to clearly localized anthropogenic impact, likely connected to the use
610 of fire (abundant micro- and macrocharcoal, Fig. 10), maybe for pastoral use. Additionally, the rise of
611 fine volcanic sediment input (rise of Sediment Accumulation Rate –SAR– and Fe/Ca ratio, lower D50)
612 suggests increased anthropogenic impacts affecting soils of the catchment slopes. This is consistent
613 with archaeological data, which show development of agglomerations on the hilltops of Limagne at
614 the end of the Bronze Age (3100-2750 cal BP), whereas slopes and lowlands seem devoted to
615 agricultural and pastoral activities (Couderc, 2019).

616 During later phases of the first Iron Age (2600-2375 cal BP, phase N2.6A and beginning of
617 N3.3A in Fig. 10, see also Fig. 11) the situation was radically different: abrupt pedo-hydrological
618 changes affected the basin since c. 2600 cal BP. The environment became much drier and landscape
619 opened further as clearly indicated by malacological assemblages. Soils became cumulic and
620 isohumic in the depression with residual hydromorphic features due to seasonal short flooding
621 episodes as indicated by micromorphology and malacological assemblages. Moreover, they present
622 micromorphological (microstructure, porosity, organic matter, pedofeatures, etc.), sedimentological
623 (OM rate increments in both cores) and malacological (reduced biodiversity) evidences of major
624 anthropogenic-induced modifications and impacts, consistent with local agricultural use starting
625 from c. 2600 cal BP. Additionally, SAR rises strongly especially in lower areas of the basin with
626 predominance of fine volcanic sediment, suggesting that erosion of soils of the catchment had similar
627 intensity to the previous period, but became more generalized (grain-size and Fe/Ca ratio, Fig. 10).

1
2
3 628 Taken together, these data clearly indicate a strong spatial expansion of agricultural impacts on soils
4
5 629 in this catchment of southern Limagne, affecting for the first time the wet lowlands c. 2600 cal BP. It
6
7 630 is noteworthy that similar phenomena are noted in the Rhone valley or in Rhineland also at the
8
9 631 beginning of the Iron Age (Houben et al., 2012; Notebaert and Berger, 2014). This expansion
10
11 632 necessarily implied a new technical capacity to drain and cultivate wetlands at least two centuries
12
13 633 before than usually admitted in Limagne (Trément et al., 2007a; Trément, 2011). This early drainage
14
15 634 capacity certainly represented a break in the socio-environmental interaction in the Limagne
16
17 635 lowlands hitherto unsuspected, and a major step towards environmental systems anthropization.
18
19 636 Even if needing confirmation through additional investigations, this precocity is not out of place since
20
21 637 drainage capacity was likely developed from the beginning of the Iron Age in central France, allowing
22
23 638 hydraulic developments and small settlements on former wetlands (Bernigaud et al., 2014; Milcent
24
25 639 and Mennessier-Jouannet, 2007; Riquier et al., 2015; Walsh et al., 2019). Remarkably, the emergence
26
27 640 of a proto-urban settlement including hundreds of storage pits in the neighboring Puy de Corent
28
29 641 takes place only few decades (from c. 2550 cal. BP) after the beginning of impacts on soils noted at la
30
31 642 Narse wet lowlands (Mayoral et al., 2018b; Milcent et al., 2014), and is maybe related to locally
32
33 643 increased agricultural production.
34
35
36
37
38
39
40
41
42
43
44
45
46
47
48
49
50
51
52
53
54
55
56
57
58
59
60

Figure 10. Multi-proxy synthetic diagram for NAR2 (A) and NAR3 (B) cores (MS: Magnetic Susceptibility. D50: median grain-size. SAR: Sediment Accumulation Rate. OM: Organic Matter content).

Accepted Manuscript

4.4 Late Iron Age

All proxies suggest that environmental dynamics at La Narse de la Sauvetat during the Late Iron Age (2375-1980 cal BP, phases 2.6B to E and N3.3A and B in Fig. 10, see also Fig. 11) were broadly similar to the previous centuries, with soil cultivation, use of fire and probable drainage works. Increased fine sediment inputs into the basin, together with micromorphological and geochemical evidence of intensified fires and soil erosion, indicate that agricultural impact on soils of the catchment became gradually more generalized and reached a maximum between 2250 and 2150 cal BP.

From 2250 cal BP onwards and until the end of the Iron Age, micromorphological and malacological data suggest that despite generally drier soils across the basin, hydrological conditions were slightly unstable. Short floods were more frequent, even if limited to the lower part of the basin, particularly between 2150 and 2050 cal BP. The reduced energy of sedimentary inputs and a decrease in volcanic fraction indicated by sedimentological and geochemical proxies, together with a reduced accumulation rate suggest a gradually reduced connectivity with catchment slopes.

Local socio-environmental dynamics at la Narse de la Sauvetat are roughly consistent with increased anthropogenic impacts noted in previous works on Limagne. For the last centuries of the Iron Age, human impact in environmental systems became strong and generalized (Ballut, 2000; Ballut and Guichard, 2005; Trément et al., 2007a; Trément, 2011), while climatic conditions were more favorable to agricultural activities during the Roman Warm Period (Magny, 2004 ; McCormick et al., 2012). Reduction of sedimentary inputs into the basin could be connected with the emergence and development of new agricultural practices in Limagne, such as improved drainage networks or terraced fields on the slopes (Ballut and Guichard, 2005; Trément et al., 2007a; Trément, 2011). These anthropogenic modifications of hydro-sedimentary systems may have significantly contributed to contain soil erosion and hydro-sedimentary degradation.

4.5 Antiquity

The Roman epoch (1980 to 1474 cal. BP, phases N2.6E to N2.7B and N.3.3B to N3.4B, Fig. 10, see also Fig. 11) appears to be a very strong anthropogenic impact period in the basin. Soil micromorphology, relatively high OM content and malacology indicate more intensive agriculture and an improved drainage. Several Pb/Rb peaks in both cores (Fig. 10), not correlated with detrital inputs, indicate local metallurgical activity from c. 1950 cal BP to c. 1600 cal BP. The maintained decrease of SAR in the basin and the soil profile stability during the Early Roman Empire (incipient illuviation, Fig. 6) can be interpreted as a strong control of hydro-sedimentary inputs. A pronounced deterioration and anthropogenic erosion of volcanic soils of the catchment can nevertheless be deduced from the increased number of coarse volcanic particles and the geochemical composition of fine fraction (high values of Fe/Ca since c. 1800 cal BP). Impacts on soils and especially on hydro-sedimentary system became more evident after 1700 cal BP, with micromorphological data suggesting more fluctuant hydrological conditions and high detrital inputs from volcanic slopes (Fe/Ca, Fig.10).

These environmental data are consistent with local archaeological evidence, with several Roman settlements (including a very extended *villa*) indicating increased human impacts in La Narse de la Sauvetat basin (Simon et al., 2017), similar to the neighboring Sarliève palaeolake (Fourmont, 2006 ; Trément et al., 2007a; Trément, 2011; Vernet, 2001; Vernet et al., 2005). At a regional level, human impact on natural systems also became very strong during the Roman period (Ballut and Guichard, 2005; Berger, 2015; Notebaert and Berger, 2014). Hydro-sedimentary and soil degradation after 1700 cal BP could be linked to a short phase of colder and drier climate between 1750 and 1650 cal BP, which was followed by relatively unstable hydro-climatic conditions (Buntgen et al., 2011; Holzhauser et al., 2005). However, resilience of Late Roman Empire agrarian structures probably allowed settlers to contain sedimentary inputs into the basin, or efficiently evacuate them through a drainage network.

Figure 11. Comparison of palaeoenvironmental evidence in la Narse de la Sauvetat between 5000 and 1200 cal BP (derived from core NAR2, this study) with regional archaeological data in Limagne plain and climatic changes in Western Europe. NAR2 environmental phases are from Fig. 10A. Representations of local hydrological conditions, soil erosion in the catchment and detrital inputs are qualitative (relative level or thickness according to process intensity) and based on data from Fig. 10. High-energy hydro-sedimentary episodes related to 4.2 and 3.5 kyr. cal BP climatic events are indicated (note a chronological offset of 150-200 yr. of the first episode, see the text for details). Local vegetation cover (qualitative) is represented by the proportion of shade-demanding malacological species vs. other terrestrial malacological species. Anthropogenic activities (landscape opening, use of fire, pastoral activity, agriculture and metallurgical activity) are represented by symbols. RWP: Roman Warm Period. LALIA: Late Antiquity Little Ice Age. Settlement density in Limagne is based on (1) Ballut and Argant, 2004; Couderc, 2019; Daugas and Raynal, 1989; Milcent and Mennessier-Jouannet, 2007; Raynal et al., 2003; Trément et al., 2007; Trément, 2011. Phases of climatic deterioration in Western Europe are based on (2) Berger et al., 2007; Brisset et al., 2013; Buntgen et al., 2011; Carozza et al., 2015; Fletcher, Debret and Goñi, 2013; Holzhauser et al., 2005; Joerin et al., 2006; Magny, 2004; Magny et al., 2009; McCormick et al., 2012; Van Geel and Magny, 2002; Walker et al., 2019; Walsh et al., 2019.

4.6 Late Antiquity and early Middle Ages

The transition from Antiquity to the early Middle Ages (1500 to 1200 cal BP, N2.8A to C and N3.4A to N3.5, Fig. 10, see also Fig. 11) is characterized by a major palaeoenvironmental change at la Narse de la Sauvetat, starting from c. 1500 cal BP with sudden deposition of a black, organic and charcoal-rich layer. Based on geochemical, micromorphological and malacological data, this deposit has been interpreted as a marsh resulting from flooding of the lower areas of the depression whereas open landscape was maintained in drier peripheral areas. Detrital inputs were reduced (lower MS, low SAR), but remained relatively rich in volcanic fraction (Fe/Ca).

This palustrine phase was very similar to the well-known “dark layer” of the Sarliève palaeolake a few kilometers north, dated approximately between 1850 and 1750 cal BP. That layer has been interpreted as the result of introduction in hillslopes of the catchment of new pastoral practices involving fire combined with a late-Antiquity hydro-climatic degradation (Buntgen et al., 2011; Trément et al., 2007a; Trément, 2011; Vernet, 2001; Vernet et al., 2005). However, the dark layer observed at la Sauvetat has a 300-year chronological offset respect the Sarliève one: this strongly suggests that this major change had little to do with climate excursions, but was more likely due to modifications of anthropogenic activities on the catchment, implying sudden deterioration of drainage networks or even outlet modifications.

Moreover, the strong hydro-sedimentary “crisis” sometimes noted in Limagne from 1550 or 1450 cal BP in previous works and often attributed to socio-climatic drivers (Ballut, 2001; Ballut and Guichard, 2005; Trément et al., 2007a, 2007b; Vernet, 2013), is remarkably absent here. This suggests that, at least locally, late Antiquity landscape changes, due to modifications in anthropic activities and in land management, were gradual and controlled instead of abrupt and catastrophic. Spatial reorganizations and differential land use can explain these environmental variations at the micro-regional scale. Similar dynamics of land-use changes in wet lowlands during Late Antiquity or early Middle Ages have been identified by palaeoenvironmental research in SE France, and are likely connected with hydraulic systems abandonment (Berger, 1995; Durand & Leveau, 2004), but the question remains nevertheless obscure in Limagne and would require further investigations.

The picture between 1400 and 1300 cal BP is less ambiguous as water level rose in the basin: lower areas became clearly aquatic (with in situ travertine formation) and palustrine environments prograded to the margins of the depression. This marked drainage deterioration is also noted in other Limagne marshy areas (Trément, 2011; Vernet et al, 2005; Vernet, 2013), and was followed by slightly dryer conditions after 1300 cal BP. Strong hydro-climatic phenomena are locally noted in Limagne by scarce but reliable historical sources mentioning increased floods and seismicity (Daugas and Tixier, 1975; Vernet, 2011; Vernet, 2013). These dynamics are in accord with hydro-climatic degradation between 1450 and 1250 cal BP, which is well documented at western European scale (Arnaud et al., 2012; Berger and Brochier, 2006; Buntgen et al., 2011; Magny, 2004; McCormick et al., 2012). The influence of new forms of human management on this wetland remains nevertheless difficult to assess based only on these palaeoenvironmental insights, and further research is necessary to better understand socio-environmental interaction driving the early medieval landscape changes at la Narse de la Sauvetat.

5-Conclusion

1
2
3 753 This work used multi-proxy geoarchaeological and palaeoenvironmental analysis to reconstruct
4
5 754 landscape evolution and human-environment interactions at La Narse de la Sauvetat.
6
7 755 Micromorphological, geochemical, sedimentological and malacological data supported by a robust
8
9 756 chronological framework allowed for the first time in Limagne lowlands a precise discussion
10
11 757 concerning the weight of anthropogenic and climatic drivers on pedo-hydro-sedimentary processes
12
13 758 and landscape evolution of the basin from Late Neolithic to the early Middle Ages.
14
15
16

17 759 The Late Neolithic was poorly documented in the pedo-sedimentary analyzed records, but
18
19 760 nevertheless anthropogenic modifications of vegetation cover could be discerned. Until the Middle
20
21 761 Bronze Age, hydro-sedimentary dynamics in the depression were strong and clearly climate-driven by
22
23 762 the 4.2 and 3.5 kyr cal BP climate events, characterized for the first time in Limagne lowlands. The
24
25 763 first clear evidences of incipient anthropogenic impact in soils of the basin and the catchment
26
27 764 appeared in the Late Bronze Age, under slightly better hydro-climatic conditions.
28
29
30

31 765 However the decisive phase in human impact affecting soil erosion, hydro-sedimentary system and
32
33 766 wet areas of the catchment occurred at the opening of the Iron Age. Despite probably less favorable
34
35 767 climatic conditions during some centuries after 2750 cal BP, agricultural impacts on soils of the basin
36
37 768 became evident c. 2600 cal BP and were probably accompanied by drainage works, as soil erosion in
38
39 769 the catchment rose.
40
41
42

43 770 Hallstatt societies seemed therefore to have acquired a first degree of emancipation from hydro-
44
45 771 climatic constraints affecting these wet lowlands, crossing a major threshold in socio-environmental
46
47 772 interaction in southern Limagne. This precocious forcing of soils and hydro-sedimentary system
48
49 773 occurred considerably earlier than the Late Iron Age turning point (2250-2050 cal BP) usually
50
51 774 accepted in Limagne. These dynamics were reinforced during La Tène and Roman periods, and
52
53 775 impact on soils and hydro-sedimentary system expanded and deepened. However after reaching a
54
55 776 peak c. 2200 cal BP the hydro-sedimentary consequences of rising anthropogenic impact appeared to
56
57 777 decrease. This is probably due to improved land management and agricultural techniques including
58
59
60

778 hydraulics, allowing more efficient management and containment of erosion processes. Despite
779 rather favorable climatic conditions, a disruption in hydro-sedimentary system became gradually
780 discernible throughout the Roman period and especially during the Late Roman Empire. This signal
781 could be due to more unstable climatic conditions contributing to upset an anthropogenic
782 environmental system with centuries of cumulative impacts.

783 Sudden drainage degradation and the advent of palustrine conditions in the basin from 1500 cal BP
784 were remarkably asynchronous with other similar local dynamics. They were probably more the
785 result of modifications of land management rather than of hydro-climatic degradation that occurred
786 anyway a century later. These results go against the idea of a dramatic “collapse” of late Antiquity
787 socio-environmental systems in southern Limagne, drawing a more complex picture. They rather
788 indicate that, at least locally, their relative resilience could have allowed a fast but nevertheless
789 gradual transition to a new equilibrium in the early Middle Ages, characterized by abandonment of
790 drainage networks and occupation of lowlands by lacustro-palustrine environments under oscillating
791 climatic conditions.

792 Ultimately, this work confirmed that multi-proxy, high resolution analysis is the most fruitful
793 approach to develop in Limagne lowlands, where the interpretation of socio-environmental
794 interaction based on palaeoenvironmental record of soils and wetlands had long been limited. The
795 obtained results, partly consistent with previous knowledge, raised specific questions due to
796 increased chronological and analytical resolution, which would be regionally addressed by further
797 multi-disciplinary research.

798 **6-Acknowledgements**

799 This work was carried out as a part of the AYPONA project (Dir. Y. Miras and F. Vautier) funded by the
800 Conseil Régional d’Auvergne (Fr.). Analyses were funded by University Lyon 2 (Projet BQR - University
801 Lyon 2, dir. M. Poux and J-F. Berger). Coring was performed with financial support of the Zone Atelier

Loire. The authors want to acknowledge the landowners M. Favy and M. De Quatrebarbes who allowed access to their fields. We are also grateful to a number of persons who contributed to this work with their support in the field, with laboratory assistance, or with valuable scientific discussions: Aude Beauger, Erwan Roussel, Alexandre Garreau, François-Xavier Simon, Alexandre Poiraud, Laura Benedito, Pierre Boivin, Franck Vautier, Bertrand Dousteyssier, Florian Couderc, Olivier Voldoire, Paul Ledger, Manon Cabanis, Fayçal Soufi and Adrien Barra. Lastly, we express sincere thanks to the reviewers for their critical reading of the manuscript and constructive remarks.

7-Conflicts of interest

The authors declare no conflict of interest. The founding sponsors had no role in the design of the study; in the collection, analyses, or interpretation of data; in the writing of the manuscript, and in the decision to publish the results.

8-References

- Adderley WP, Wilson CA, Simpson IA, et al. (2010) Anthropogenic Features. In: *Interpretation of Micromorphological Features of Soils and Regoliths*. Elsevier, pp. 569–588. DOI: 10.1016/B978-0-444-53156-8.00025-8.
- Arnaud F, Revel-Rolland M, Bosch D, et al. (2004) A 300 year history of lead contamination in northern French Alps reconstructed from distant lake sediment records. *Journal of Environmental Monitoring* 6(5): 448–456. DOI: 10.1039/b314947a.
- Arnaud F, Serralongue J, Winiarski T, et al. (2006) Pollution au plomb dans la Savoie antique (II–IIIe s. apr. J.-C.) en relation avec une installation métallurgique de la cité de Vienne. *Comptes Rendus Geoscience* 338(4): 244–252. DOI: 10.1016/j.crte.2005.11.008.
- Arnaud F, Révillon S, Debret M, et al. (2012) Lake Bourget regional erosion patterns reconstruction reveals Holocene NW European Alps soil evolution and paleohydrology. *Quaternary Science*

- 825 *Reviews* 51. Elsevier Ltd: 81–92. DOI: 10.1016/j.quascirev.2012.07.025.
- 826 Bajard M, Sabatier P, David F, et al. (2015) Erosion record in Lake La Thuile sediments (Prealps,
827 France): Evidence of montane landscape dynamics throughout the Holocene. *The Holocene*
828 26(3): 350–364. DOI: 10.1177/0959683615609750.
- 829 Ballut and Argant J (2004) Les dynamiques géomorphologiques et environnementales dans la
830 Limagne humide de Clermont-Ferrand du Néolithique au début de l'Age du Fer. In: *5e*
831 *Rencontres méridionales de Préhistoire récente Auvergne et Midi*, Clermont-Ferrand, 2004.
- 832 Ballut C (2000) *Evolution environnementale de la Limagne de Clermont-Ferrand au cours de la*
833 *seconde moitié de l'holocène (Massif central français)*. Université de Limoges. Available at:
834 <http://www.theses.fr/2000LIMO2004>.
- 835 Ballut C (2001) Evolution géomorphologique et hydrologique dans les marais de Limagne au cours de
836 la seconde moitié de l' Holocène (Massif central , France) / Geomorphological and
837 hydrological evolution in the Limagne swamps during the second part of the Holocene.
838 *Quaternaire* 12(1–2): 43–51.
- 839 Ballut C and Guichard V (2005) Anthropisation et milieu humide en Limagne de Clermont-Ferrand
840 depuis le Neolithique. In: *Occupation et gestion des plaines alluviales dans le Nord de la France*
841 *de l'âge du Fer à l'époque gallo-romaine* (ed. C Petit), Besançon, 2005, pp. 135–141. Presses
842 Universitaires de Franche-Comté.
- 843 Berger, Brochier JL, Vital J, et al. (2007) Nouveau regard sur La dynamique des paysages et
844 l'occupation humaine à L'Âge du Bronze en moyenne vallée du Rhône. In: *Environnements et*
845 *cultures à l'Age du bronze en Europe occidentale* (eds H Richard, C Mordant, and M Magny),
846 Paris, 2007, p. 399. Editions du CTHS.
- 847 Berger J-F (1995) Facteurs anthropiques et naturels de l'évolution des paysages romains et

- 848 protomédiévaux du Bassin valdainais (Drôme). *L'homme et la dégradation de l'environnement*.
- 849 *XVèmes Rencontres Internationales d'Archéologie et d'Histoire d'Antibes*. Editions APDCA, Juan-
- 850 les-Pins: 79–114.
- 851 Berger J-F and Brochier J-L (2006) Paysages et climats en moyenne vallée du Rhône : apports de la
- 852 géoarchéologie. In: *Habitats, Nécropoles et Paysages Dans La Moyenne et Basse Vallée Du*
- 853 *Rhône (VIIe-XVe s.). Contribution Des Travaux Du TGV-Méditerranée à l'étude Des Sociétés*
- 854 *Rurales Médiévales*. Documents d'Archéologie Française, pp. 163–208.
- 855 Berger J-F, Shennan S and Woodbridge J (2019) Holocene land cover and population dynamics in
- 856 Southern France. *The Holocene*: 31–34. DOI: 10.1177/0959683619826698.
- 857 Berger J (2015) *Approche socio-environnementale du Néolithique à l'Anthropocène : quelques études*
- 858 *intégrées de la Vallée du Rhône aux milieux Nord Méditerranéens. Habilitation à Diriger les*
- 859 *Recherches*. Université de Lyon 2.
- 860 Berger JF, Delhon C, Magnin F, et al. (2016) A fluvial record of the mid-Holocene rapid climatic
- 861 changes in the middle Rhone valley (Espeluche-Lalo, France) and of their impact on Late
- 862 Mesolithic and Early Neolithic societies. *Quaternary Science Reviews* 136: 66–84. DOI:
- 863 10.1016/j.quascirev.2015.11.019.
- 864 Bernigaud N, Berger J-F, Bouby L, et al. (2014) Ancient canals in the valley of Bourgoin-La Verpillière
- 865 (France, Isère): morphological and geoarchaeological studies of irrigation systems from the Iron
- 866 Age to the Early Middle Ages (8th century bc–6th century ad). *Water History* 6(1): 73–93. DOI:
- 867 10.1007/s12685-013-0096-9.
- 868 Birks HH and Birks HJB (2006) Multi-proxy studies in palaeolimnology. *Vegetation History and*
- 869 *Archaeobotany* 15(4). Springer-Verlag: 235–251. DOI: 10.1007/s00334-006-0066-6.
- 870 Blaauw M (2010) Methods and code for 'classical' age-modelling of radiocarbon sequences.

- 871 *Quaternary Geochronology* 5(5). Elsevier: 512–518. DOI: 10.1016/J.QUAGEO.2010.01.002.
- 872 Blott SJ and Pye K (2001) Gradistat: A Grain Size Distribution and Statistics Package for the Analysis of
873 Unconsolidated Sediments. *Earth Surface Processes and Landforms* 26: 1237–1248. DOI:
874 10.1002/esp.261.
- 875 Bornand M, Callot G, Favrot J-C, et al. (1968) Les sols du Val d'Allier, notice explicative de la carte
876 pédologique au 1/100.000ème. Montpellier: INRA, Service d'étude des sols.
- 877 Bouiller R (1979) Minute de la carte Géologique de la France à 1:50000, feuille 717 (Veyre-Monton).
878 BRGM.
- 879 Bravard J-P and Peiry J-L (1999) The CM pattern as a tool for the classification of alluvial suites and
880 floodplains along the river continuum. *Floodplains: Interdisciplinary Approaches* 163(1969):
881 259–268. DOI: 10.1144/GSL.SP.1999.163.01.20.
- 882 BRGM (1973) *Carte Geologique 1/50.000 N°693 (Clermont-Ferrand)*. BRGM (ed.). Orléans: BRGM.
- 883 Brisset E, Miramont C, Guiter F, et al. (2013) Non-reversible geosystem destabilisation at 4200 cal.
884 BP: Sedimentological, geochemical and botanical markers of soil erosion recorded in a
885 Mediterranean alpine lake. *Holocene* 23(12): 1863–1874. DOI: 10.1177/0959683613508158.
- 886 Brown A, Toms P, Carey C, et al. (2013) Geomorphology of the Anthropocene: Time-transgressive
887 discontinuities of human-induced alluviation. *Anthropocene* 1. Elsevier B.V.: 3–13. DOI:
888 10.1016/j.ancene.2013.06.002.
- 889 Brown AG, Tooth S, Bullard JE, et al. (2016) The geomorphology of the Anthropocene: emergence,
890 status and implications. *Earth Surface Processes and Landforms* 42(1): 71–90. DOI:
891 10.1002/esp.3943.
- 892 Buntgen U, Tegel W, Nicolussi K, et al. (2011) 2500 Years of European Climate. *Science* 331(February):
893 578–582.

- 894 Burga CA, Perret R and Zoller H (2001) Swiss localities of early recognized Holocene climate
 895 oscillations: Characterization and significance. *Vierteljahrsschrift der Naturforschenden*
 896 *Gesellschaft in Zuerich* 146(2–3): 65–74.
- 897 Carozza L, Berger J, Burens A, et al. (2015) Society and environment in Southern France from the 3rd
 898 millenium BC to the beginning of the 2d millenium BC a tipping point? In: *2200 BC – Ein*
 899 *Klimasturz Als Ursache Für Den Zerfall Der Alten Welt ? 2200 BC – A Climatic Breakdown as a*
 900 *Cause for the Collapse of the Old World ?*, pp. 833–844.
- 901 Chassiot L, Miras Y, Chapron E, et al. (2018) A 7000-year environmental history and soil erosion
 902 record inferred from the deep sediments of Lake Pavin (Massif Central, France).
 903 *Palaeogeography, Palaeoclimatology, Palaeoecology* 497(February). Elsevier: 218–233. DOI:
 904 10.1016/j.palaeo.2018.02.024.
- 905 Couderc F (2019) La basse Auvergne (Puy-de-Dôme, sud Allier) : un espace privilégié pour l'étude des
 906 territoires et des paysages de l'âge du Bronze. In: *Colloque international anniversaire de l'*
 907 *APRAB*, Bayeux, 2019, pp. 94–97. APRAB.
- 908 Courty M-A, Goldberg P and MacPhail RI (1989) *Soils and Micromorphology in Archaeology*.
 909 *Cambridge manuals in archaeology*. DOI: 10.1016/B978-0-444-53156-8.00031-3.
- 910 Croudace IW and Rothwell RG (2015) *Micro-XRF Studies of Sediment Cores*. New York London:
 911 Springer. DOI: 10.1007/978-1-4020-5725-0_3.
- 912 Crutzen PJ and Stoermer EF (2000) The 'Anthropocene'. *Global Change Newsletter* 41(41): 17–18.
 913 Available at:
 914 <http://www.igbp.net/publications/globalchangemagazine/globalchangemagazine/globalchange>
 915 [newslettersno4159.5.5831d9ad13275d51c098000309.html](http://www.igbp.net/publications/globalchangemagazine/globalchangemagazine/globalchange).
- 916 Daugas and Raynal JP (1989) Quelques étapes du peuplement du Massif central français dans leur

- 917 contexte paléoclimatique et paléogéographique Some stages of prehistoric settlement in Massif
918 Central. *Cahiers du Quaternaire* 13: 67–95.
- 919 Daugas J-P and Tixier L (1977) Variations paleoclimatiques de la Limagne d’Auvergne. *Approche*
920 *écologique de l’Homme Fossile, supplément au Bulletin de l’AFEQ* 47: 203–235.
- 921 Daugas J and Tixier L (1975) Variations Paléoclimatiques de la Limagne d’Auvergne. *Bulletin de*
922 *l’Association française pour l’étude du Quaternaire* 47: 203–235.
- 923 Deák J, Magny M and Wüthrich S (2017) Late Neolithic to Middle Bronze Age (around 4900–3100 cal.
924 BP) lake-level fluctuations at Lake Neuchâtel (Switzerland) as reflected by the sediment
925 sequence of the site of Colombier/Les Plantées de Rive: Palaeoclimatic and archaeological
926 implications. *Holocene* 28(1): 3–18. DOI: 10.1177/0959683617714598.
- 927 Deák J, Gebhardt A, Lewis H, et al. (2017) Soils Disturbed by Vegetation Clearance and Tillage. In:
928 *Archaeological Soil and Sediment Micromorphology*. Chichester, UK: John Wiley & Sons, Ltd, pp.
929 231–264. DOI: 10.1002/9781118941065.ch28.
- 930 Dearing J (1999) Magnetic susceptibility. *Environmental magnetism: A practical guide* 6. Quaternary
931 Research Association, London, Technical Guide: 35–62.
- 932 Delvigne J (1998) *Atlas of Micromorphology of Mineral Alteration and Weathering. The canadian*
933 *Mineralogist*. Available at: <http://petrology.oxfordjournals.org/content/41/3/475.2.short>.
- 934 Demény A, Kern Z, Czuppon G, et al. (2019) Middle Bronze Age humidity and temperature variations,
935 and societal changes in East-Central Europe. *Quaternary International* 504(November): 80–95.
936 DOI: 10.1016/j.quaint.2017.11.023.
- 937 Dotterweich M (2013) The history of human-induced soil erosion: Geomorphic legacies, early
938 descriptions and research, and the development of soil conservation—A global synopsis.
939 *Geomorphology* 201. Elsevier B.V.: 1–34. DOI: 10.1016/j.geomorph.2013.07.021.

- 940 Dreibrodt S, Lubos C, Terhorst B, et al. (2010) Historical soil erosion by water in Germany: Scales and
 941 archives, chronology, research perspectives. *Quaternary International* 222(1–2). Elsevier Ltd:
 942 80–95. DOI: 10.1016/j.quaint.2009.06.014.
- 943 Durand A and Leveau P (2004) FARMING IN MEDITERRANEAN FRANCE AND RURAL SETTLEMENT IN
 944 THE LATE ROMAN AND EARLY MEDIEVAL PERIODS : THE CONTRIBUTION FROM ARCHAEOLOGY
 945 AND ENVIRONMENTAL SCIENCES IN THE LAST TWENTY YEARS. In: Barceló M and Sigaut F (eds)
 946 *The Making of Feudal Agricultures*. BRILL, pp. 177–253.
- 947 Durand N, Monger HC and Canti MG (2010) Calcium Carbonate Features. In: *Interpretation of*
 948 *Micromorphological Features of Soils and Regoliths*. Elsevier, pp. 149–194. DOI: 10.1016/B978-
 949 0-444-53156-8.00009-X.
- 950 Ellis EC, Kaplan JO, Fuller DQ, et al. (2013) Used planet: A global history. *Proceedings of the National*
 951 *Academy of Sciences* 110(20): 7978–7985. DOI: 10.1073/pnas.1217241110.
- 952 Ellis EC, Magliocca NR, Stevens CJ, et al. (2017) Evolving the Anthropocene: linking multi-level
 953 selection with long-term social–ecological change. *Sustainability Science* 13(1). Springer Japan:
 954 119–128. DOI: 10.1007/s11625-017-0513-6.
- 955 Evans JG (1972) *Land Snails in Archaeology; with Special Reference to the British Isles*. Seminar Press.
 956 Available at: https://books.google.fr/books/about/Land_Snails_in_Archaeology.html?id=Yg_AAAIAAJ&redir_esc=y (accessed 29 January 2019).
- 958 Fedoroff N and Courty M-A (2002) Paléosols et sols reliques. *Miskovsky JC Géologie de la préhistoire,*
 959 *Association pour l'étude de l'environnement géologique de la préhistoire, Paris: 277–316.*
- 960 Fedoroff N, Courty M-A and Guo Z (2010) Palaeosoils and Relict Soils. In: *Interpretation of*
 961 *Micromorphological Features of Soils and Regoliths*. Elsevier, pp. 623–662. DOI: 10.1016/B978-
 962 0-444-53156-8.00027-1.

- 963 Fernández-Götz M (2018) Urbanization in Iron Age Europe: Trajectories, Patterns, and Social
 964 Dynamics. *Journal of Archaeological Research* 26(2): 117–162. DOI: 10.1007/s10814-017-9107-
 965 1.
- 966 Fletcher WJ, Debret M and Sanchez-Goñi M-F (2013) Mid-Holocene emergence of a low-frequency
 967 millennial oscillation in western Mediterranean climate: Implications for past dynamics of the
 968 North Atlantic atmosphere westerlies. *The Holocene*: 1–14. DOI: 10.1177/0959683612460783.
- 969 Fletcher WJ, Debret M and Goñi MFS (2013) Mid-Holocene emergence of a low-frequency millennial
 970 oscillation in western Mediterranean climate: Implications for past dynamics of the North
 971 Atlantic atmospheric westerlies. *The Holocene* 23(2). SAGE PublicationsSage UK: London,
 972 England: 153–166. DOI: 10.1177/0959683612460783.
- 973 Fourmont A (2006) *Quantification de l'érosion et de la sédimentation dans le bassin de Sarliève*
 974 *(Massif Central, France) au tardiglaciaire et à l'Holocène : Impact des facteurs naturels et*
 975 *anthropiques*. Université François Rabelais-Tours. Available at:
 976 <http://www.theses.fr/2005TOUR4033>.
- 977 Fourmont A, Macaire JJ and Bréhéret JG (2009) Contrasted Late Glacial and Holocene hydrology of
 978 Sarliève paleolake (France) from sediment geometry and detrital versus biochemical
 979 composition. *Journal of Paleolimnology* 41(3): 471–490. DOI: 10.1007/s10933-008-9238-y.
- 980 Freytet P and Verrecchia EP (1998) Freshwater organisms that build stromatolites: a synopsis of
 981 biocrystallization by prokaryotic and eukaryotic algae. *Sedimentology* 45(3): 535–563. DOI:
 982 10.1046/j.1365-3091.1998.00155.x.
- 983 Gebhardt A, Occhietti S and Fechner K (2014) Grandes phases de pédogenèse, d'érosion et
 984 d'anthropisation des sols au cours de la seconde moitié de l'Holocène en Lorraine.
 985 *ArchéoSciences* 38: 7–29.

- 986 Gerasimova M and Lebedeva-Verba M (2010) Topsoils – Mollic, Takyric and Yermic Horizons. In:
- 987 *Interpretation of Micromorphological Features of Soils and Regoliths*. Elsevier, pp. 351–368.
- 988 DOI: 10.1016/B978-0-444-53156-8.00016-7.
- 989 Goudie A and Viles HA (2016) *Geomorphology in the Anthropocene*. Cambridge: Cambridge
- 990 University Press.
- 991 Greffier G, Restituto J and Héraud H (1980) Aspects géomorphologiques et stabilité des versants au
- 992 sud de Clermont-Ferrand. *Bulletin de liaison du Laboratoire des Ponts et Chaussées* 107: 17–26.
- 993 Guilloré P (1980) *Méthode de Fabrication Mécanique et En Série Des Lames Minces*. 2ème édit. Paris,
- 994 Grignon: CNRS et INA-PG.
- 995 Heiri O, Lotter AF and Lemcke G (2001) Loss on ignition as a method for estimating organic and
- 996 carbonate content in sediments: reproducibility and comparability of results. *Journal of*
- 997 *Paleolimnology* 25(1). Kluwer Academic Publishers: 101–110. DOI: 10.1023/A:1008119611481.
- 998 Holzhauser H, Magny M and Zumbühl HJ (2005) Glacier and lake-level variations in west-central
- 999 Europe over the last 3500 years. *Holocene* 15(6): 789–801. DOI: 10.1191/0959683605hl853ra.
- 1000 Horsák M, Juříčková L and Picka J (2013) *Měkkýši České a Slovenské Republiky = Molluscs of the Czech*
- 1001 *and Slovak Republics*. Available at: [https://www.nhbs.com/molluscs-of-the-czech-and-slovak-](https://www.nhbs.com/molluscs-of-the-czech-and-slovak-republics-mkkyi-eske-a-slovenske-republiky-book)
- 1002 [republics-mkkyi-eske-a-slovenske-republiky-book](https://www.nhbs.com/molluscs-of-the-czech-and-slovak-republics-mkkyi-eske-a-slovenske-republiky-book) (accessed 29 January 2019).
- 1003 Houben P, Schmidt M, Mauz B, et al. (2012) Asynchronous Holocene colluvial and alluvial
- 1004 aggradation: A matter of hydrosedimentary connectivity. *The Holocene* 23(4): 544–555. DOI:
- 1005 10.1177/0959683612463105.
- 1006 Jeffery S, Gardi C, Jones A, et al. (2010) *European Atlas of Soil Biodiversity. Chart*. English Ed.
- 1007 Luxembourg: JRC-European Commission. DOI: 10.1016/S0016-7061(99)00028-2.
- 1008 Joerin UE, Stocker TF and Schlüchter C (2006) Multicentury glacier fluctuations in the Swiss Alps

- 1009 during the Holocene. *The Holocene* 16(5): 697–704. DOI: 10.1191/0959683606hl964rp.
- 1010 Joly D, Brossard T, Cardot H, et al. (2010) Les types de climats en France, une construction spatiale -
- 1011 Types of climates on continental France, a spatial construction. *Cybergéo : European Journal of*
- 1012 *Geography* (501): 1–23. DOI: 10.4000/cybergeo.23155.
- 1013 Jongerius A (1970) Some morphological aspects of regrouping phenomena in dutch soils. *Geoderma*
- 1014 4.
- 1015 Kerney MP, Cameron RAD and Bertrand A (2006) *Guide Des Escargots et Limaces d'Europe*.
- 1016 Delachaux et Niestlé.
- 1017 Kooistra MJ and Pulleman MM (2010) Features Related to Faunal Activity. In: *Interpretation of*
- 1018 *Micromorphological Features of Soils and Regoliths*. Elsevier, pp. 397–418. DOI: 10.1016/B978-
- 1019 0-444-53156-8.00018-0.
- 1020 Kovda I and Mermut AR (2010) Vertic Features. In: *Interpretation of Micromorphological Features of*
- 1021 *Soils and Regoliths*. Elsevier, pp. 109–127. DOI: 10.1016/B978-0-444-53156-8.00007-6.
- 1022 Kühn P, Aguilar J and Miedema R (2010) Textural Pedofeatures and Related Horizons. In:
- 1023 *Interpretation of Micromorphological Features of Soils and Regoliths*. Elsevier, pp. 217–250.
- 1024 DOI: 10.1016/B978-0-444-53156-8.00011-8.
- 1025 Lang A (2003) Phases of soil erosion-derived colluviation in the loess hills of South Germany. *Catena*
- 1026 51(3–4): 209–221. DOI: 10.1016/S0341-8162(02)00166-2.
- 1027 Legrand P, Bartoli F and Curt T (2007) Spécificités des sols volcaniques du Massif Central: bénéfices et
- 1028 contraintes pour la gestion forestière. *Revue Forestière Française* 59(2).
- 1029 Lindbo DL, Stolt MH and Vepraskas MJ (2010) Redoximorphic Features. In: *Interpretation of*
- 1030 *Micromorphological Features of Soils and Regoliths*. Elsevier, pp. 129–147. DOI: 10.1016/B978-
- 1031 0-444-53156-8.00008-8.

- 1032 Loaiza JC, Stoops G, Poch RM, et al. (2015) Manual de micromorfología de suelos y técnicas
1033 complementarias. *Fondo Editorial Pascual Bravo*: 348.
- 1034 Macaire JJ, Fourmont A, Argant J, et al. (2010) Quantitative analysis of climate versus human impact
1035 on sediment yield since the Lateglacial: The Sarliève palaeolake catchment (France). *The
1036 Holocene* 20(4): 497–516. DOI: 10.1177/0959683609355181.
- 1037 MacKenzie WS, Donaldson CH and Guilford C (1982) *Atlas of Igneous Rocks and Their Textures*. ELBS.
- 1038 Macphail RI and Goldberg P (2018) *Applied Soils and Micromorphology in Archaeology*. Barker G,
1039 Slater E, and Bogucki P (eds). Cambridge: Cambridge Manuals in Archaeology-Cambridge
1040 University Press.
- 1041 Macphail RI, Courty M-A and Gebhardt A (1990) Soil Micromorphological Evidence of Early
1042 Agriculture in North-West Europe. *World Archaeology* 22(1): 53–69.
- 1043 Magny, Peyron O, Gauthier E, et al. (2009) Quantitative reconstruction of climatic variations during
1044 the Bronze and early Iron ages based on pollen and lake-level data in the NW Alps, France.
1045 *Quaternary International* 200(1–2): 102–110. DOI: 10.1016/j.quaint.2008.03.011.
- 1046 Magny M (2004) Holocene climate variability as reflected by mid-European lake-level fluctuations
1047 and its probable impact on prehistoric human settlements. *Quaternary International* 113: 65–
1048 79. DOI: 10.1016/S1040-6182(03)00080-6.
- 1049 Mayoral A (2018) *Analyse de sensibilité aux forçages anthropo-climatiques des paysages
1050 protohistoriques et antiques du plateau volcanique de Corent (Auvergne) et de ses marges par
1051 une approche géoarchéologique pluri-indicateurs*. Université Clermont Auvergne.
- 1052 Mayoral A, Peiry J-L, Berger J, et al. (2018) Geoarchaeology and chronostratigraphy of the Lac du Puy
1053 intra-urban protohistoric wetland, Corent, France. *Geoarchaeology*.
- 1054 Mayoral A, Peiry JL, Berger JF, et al. (2018) Origin and Holocene geomorphological evolution of the

- 1055 landslide-dammed basin of la Narse de la Sauvetat (Massif Central, France). *Geomorphology*
- 1056 320. Elsevier B.V.: 162–178. DOI: 10.1016/j.geomorph.2018.08.015.
- 1057 McCormick M, Büntgen U, Cane MA, et al. (2012) Climate Change during and after the Roman
- 1058 Empire: Reconstructing the Past from Scientific and Historical Evidence. *Journal of*
- 1059 *Interdisciplinary History* 43(2): 169–220. DOI: 10.1162/JINH_a_00379.
- 1060 Mielke JE (1979) Composition of the Earth's crust and distribution of the elements. *Review of*
- 1061 *research on modern problems in geochemistry*. Paris: Int. Association for Geochemistry and
- 1062 Cosmochemistry: 13–37.
- 1063 Milcent P-Y and Mennessier-Jouannet C (2007) Entre déterminisme environnemental et processus
- 1064 historiques: formes et modalités d'occupation du sol en Basse Auvergne du Bronze Final au
- 1065 début du second Age du Fer. In: Richard H, Magny M, and Mordant C (eds) *Environnements et*
- 1066 *Cultures à l'Âge Du Bronze En Europe Occidentale- Documents Préhistoriques N° 21*. Paris: CTHS,
- 1067 p. 399.
- 1068 Milcent P-Y, Poux M, Mader S, et al. (2014) Une agglomération de hauteur autour de 600 a.C. en
- 1069 Gaule centrale : Corent (Auvergne). *Transalpinare*: 181–204.
- 1070 Miras Y, Mariani M, Couderc F, et al. (2018) Addressing the complexity of the paleoenvironmental
- 1071 impact of Prehistoric settlement and Protohistoric urbanism in the Auvergne Mountains (Massif
- 1072 Central, France). In: *IEMA VOLUME-ARCHAEOLOGY OF MOUNTAIN LANDSCAPES:*
- 1073 *INTERDISCIPLINARY RESEARCH STRATEGIES OF AGRO-PASTORALISM IN UPLAND REGIONS*, 2018.
- 1074 Nehlig P, Boivin P, De Goër A, et al. (2003) Les volcans du Massif central. *Géologues (sp. issue)*: 1–41.
- 1075 Nichols K and Gogineni B (2018) The Anthropocene's dating problem: Insights from the geosciences
- 1076 and the humanities. *Anthropocene Review* 5(2): 107–119. DOI: 10.1177/2053019618784971.
- 1077 Nicosia C and Stoops G (2017) *Archaeological Soil and Sediment Micromorphology*. Wiley Blackwell.

- 1078 Notebaert, Berger JF and Brochier JL (2014) Characterization and quantification of Holocene colluvial
 1079 and alluvial sediments in the Valdaine Region (southern France). *Holocene* 24: 1320–1335. DOI:
 1080 10.1177/0959683614540946.
- 1081 Notebaert B and Berger J (2014) Quantifying the anthropogenic forcing on soil erosion during the
 1082 Iron Age and Roman Period in southeastern France. *Anthropocene* 8(2014). Elsevier B.V.: 59–69.
 1083 DOI: 10.1016/j.ancene.2015.05.004.
- 1084 Pagliai M and Stoops G (2010) Physical and Biological Surface Crusts and Seals. In: *Interpretation of*
 1085 *Micromorphological Features of Soils and Regoliths*. Elsevier, pp. 419–440. DOI: 10.1016/B978-
 1086 0-444-53156-8.00019-2.
- 1087 Passega R (1977) Significance of CM diagrams of sediments deposited by suspensions. *Sedimentology*
 1088 24(5): 723–733. DOI: 10.1111/j.1365-3091.1977.tb00267.x.
- 1089 Poux M (2012) *Corent, Voyage Au Coeur d'une Ville Gauloise*. Paris: Editions Errance.
- 1090 Poux M, Milcent P-Y, Pranyies A, et al. (2018) *Corent, Fouille pluriannuelle 2014-2016, Rapport Final*
 1091 *d'Opération*.
- 1092 Provost M and Mennessier-jouannet C (1994) Carte archéologique de la Gaule 63-2 Le Puy-de-Dôme.
 1093 Paris: Ministère de la Culture.
- 1094 Raynal J, Vernet G and Daugas J (2003) Evolution récente de la Limagne d'Auvergne (France) :
 1095 impacts du volcanisme et aspects des peuplements humains au Tardiglaciaire et à l'Holocène .
 1096 In: *Variazoni climatico-ambientali e impatto sull'uomo nell'area circum-mediterranea durante*
 1097 *l'Olocene, Territorio storico et ambiente 3* (eds C Albore-Livadie and F Ortolani), Bari, 2003, pp.
 1098 461–475. Edipuglia.
- 1099 Reimer PJ, Bard E, Bayliss A, et al. (2013) IntCal13 and Marine13 Radiocarbon Age Calibration Curves
 1100 0–50,000 Years cal BP. *Radiocarbon* 55(4): 1869–1887. DOI: 10.2458/azu_js_rc.55.16947.

- 1101 Riquier V, Auxiette G, Fechner K, et al. (2015) Éléments de géographie humaine et économique à
 1102 l'âge du Bronze et au premier âge du Fer dans la plaine de Troyes. *Bulletin de la Société*
 1103 *préhistorique française* 112(2): 339–367.
- 1104 Ruddiman WF (2003) THE ANTHROPOGENIC GREENHOUSE ERA BEGAN THOUSANDS OF YEARS AGO.
 1105 *Climatic Change* 61: 261–293. DOI: 10.1007/s10584-005-7278-0.
- 1106 Ruddiman WF (2018) Three flaws in defining a formal 'Anthropocene'. *Progress in Physical*
 1107 *Geography* 42(4): 451–461. DOI: 10.1177/0309133318783142.
- 1108 Ruddiman WF, Ellis EC, Kaplan JO, et al. (2015) Defining the epoch we live in. Is a formally designated
 1109 'Anthropocene' a good idea? *Science* 348(6230): 38–39. DOI: 10.1126/science.aaa7297.
- 1110 Sabatier P, Dezileau L, Briquieu L, et al. (2010) Clay minerals and geochemistry record from northwest
 1111 Mediterranean coastal lagoon sequence: Implications for paleostorm reconstruction.
 1112 *Sedimentary Geology* 228(3–4). Elsevier: 205–217. DOI: 10.1016/J.SEDGEO.2010.04.012.
- 1113 Salminen R, Batista MJ, Bidovec M, et al. (2005) FOREGS Geochemical Atlas of Europe, Part I*
 1114 Background Information, Methodology, and Maps. *Geol. Surv. Finland, Espoo*.
- 1115 Scholle PA and Ulmer-scholle DS (2003) *A Color Guide to the Petrography of Carbonate Rocks :*
 1116 *Grains, Texture, Porosity, Diagenesis*. Tulsa, Oklahoma: American Association of Petroleum
 1117 Geologists.
- 1118 Simon F-X, Dousteysier B, Pareilh-Peyrou M, et al. (2017) Occupation et gestion de l'espace à
 1119 l'Antiquité en marge d'un ancien centre Arverne, apports des données de prospections sur la
 1120 villa de Lieu Dieu (Puy-de-Dôme, France) et son espace périphérique. In: *Colloque*
 1121 *d'Archéométrie, GMPCA, Rennes, 2017*.
- 1122 Spek T, Waateringe WG Van, Kooistra M, et al. (2003) Formation and land-use history of celtic fields
 1123 in north-west Europe - An interdisciplinary case study at Zeijen, the Netherlands. *European*

- 1124 *Journal of Archaeology* 6(2): 141–173. DOI: 10.1177/146195710362003.
- 1125 Stolt MH and Lindbo DL (2010) Soil Organic Matter. In: *Interpretation of Micromorphological Features*
- 1126 *of Soils and Regoliths*. Elsevier, pp. 369–396. DOI: 10.1016/B978-0-444-53156-8.00017-9.
- 1127 Stoops (2003) *Guidelines for Analysis and Description of Soil and Regolith Thin Sections*. Madison,
- 1128 Wisconsin: Soil Science Society of America.
- 1129 Stoops G, Marcelino V and Mees F (2010a) *Interpretation of Micromorphological Features of Soils and*
- 1130 *Regoliths*. Amsterdam: Elsevier.
- 1131 Stoops G, Marcelino V and Mees F (2010b) Micromorphological Features and Their Relation to
- 1132 Processes and Classification. In: *Interpretation of Micromorphological Features of Soils and*
- 1133 *Regoliths*. Elsevier, pp. 15–35. DOI: 10.1016/B978-0-444-53156-8.00002-7.
- 1134 Stuiver M and Reimer PJ (1993) Extended 14C database and revised Calib 3.0 14C Age Calibration
- 1135 program. *Radiocarbon* 35(1): 215–230.
- 1136 Trément, Argant J, Bréhéret J-G, et al. (2007) Un ancien lac au pied de l'oppidum de Gergovie (Puy-
- 1137 de-Dôme). *Gallia* 64: 289–351.
- 1138 Trément F (2011) *Les Arvernes et Leurs Voisins Du Massif Central à l'Epoque Romaine-Une*
- 1139 *Archéologie Du Développement Des Territoires, Vol. I*. Clermont-Ferrand: Revue D'auvergne,
- 1140 Alliance Universitaire d'Auvergne.
- 1141 Trément F, Mennessier-Jouannet C, Argant J, et al. (2007) Le bassin de Sarliève : occupation du sol et
- 1142 paléo-environnement à l'âge du Fer. In: *L'archéologie de l'âge Du Fer En Auvergne, Actes Du*
- 1143 *XXVIIe Colloque International de l'A.F.E.A.F.* Clermont-Ferrand, pp. 385–400.
- 1144 Trément F, Argant J, Breheret J-G, et al. (2007) Un ancien lac au pied de l'oppidum de Gergovie (Puy-
- 1145 de-Dôme). *Gallia* 64: 289–351.

- 1146 Usai MR (2001) Textural Pedofeatures and Pre-Hadrian's Wall Ploughed Paleosols at Stanwix, Carlisle,
 1147 Cumbria, U.K. *Journal of Archaeological Science* 28(5): 541–553. DOI: 10.1006/jasc.2001.0609.
- 1148 Vallat P (2002) *Histoire de l'occupation du sol dans la Limagne des buttes (Puy-de-Dôme) de l'Age du*
 1149 *Fer à l'Antiquité Tardive*. Université d'Avignon et des pays du Vaucluse.
- 1150 Van Geel B and Magny M (2002) Mise en évidence d'un forçage solaire du climat à partir de données
 1151 paléoécologiques et archéologiques: la transition Subboréal Subatlantique. In: *Équilibres et*
 1152 *ruptures dans les écosystèmes durant les 20 derniers millénaires en Europe de l'Ouest* (eds H
 1153 Richard and A Vignot), Besançon, 2002, pp. 107–122. Presses Universitaires de Franche-Comté.
- 1154 Vernet Gérard (2013) La séquence sédimentaire des gravanches / gerzat enregistrement
 1155 d'événements «catastrophiques» À valeur chronologique en limagne d'auvergne (massif
 1156 central, France). *Quaternaire* 24(2): 109–127. DOI: 10.4000/quaternaire.6519.
- 1157 Vernet Gerard (2013) La séquence sédimentaire des gravanches / gerzat enregistrement
 1158 d'événements «catastrophiques» À valeur chronologique en limagne d'auvergne (Massif
 1159 Central, France). *Quaternaire* 24(2): 109–127. DOI: 10.4000/quaternaire.6519.
- 1160 Vital J (2004) Du Neolithique Final Au Bronze Moyen Dans Le Sud-Est De La France : 2200-1450 Av . J
 1161 C . *Cypselia* 15: 11–38.
- 1162 Walker M, Head MJ, Lowe J, et al. (2019) Subdividing the Holocene Series/Epoch: formalization of
 1163 stages/ages and subseries/subepochs, and designation of GSSPs and auxiliary stratotypes.
 1164 *Journal of Quaternary Science* 34(3). John Wiley & Sons, Ltd: 173–186. DOI: 10.1002/jqs.3097.
- 1165 Walsh K, Berger J-F, Roberts CN, et al. (2019) Holocene demographic fluctuations, climate and
 1166 erosion in the Mediterranean: A meta data-analysis. *The Holocene*: 095968361982663. DOI:
 1167 10.1177/0959683619826637.
- 1168 Wedepohl KH (1978) *Handbook of Geochemistry*. Springer-Verlag.

- 1169 Welter-Schultes FW (2012) *European Non-Marine Molluscs, a Guide for Species Identification =*
1170 *Bestimmungsbuch Für Europäische Land- Und Süßwassermollusken*. Gottingen: Planet Poster
1171 Editions. Available at: [https://www.nhbs.com/european-non-marine-molluscs-a-guide-for-](https://www.nhbs.com/european-non-marine-molluscs-a-guide-for-species-identification-bestimmungsbuch-fur-europaische-land-und-susswassermollusken-book)
1172 [species-identification-bestimmungsbuch-fur-europaische-land-und-susswassermollusken-book](https://www.nhbs.com/european-non-marine-molluscs-a-guide-for-species-identification-bestimmungsbuch-fur-europaische-land-und-susswassermollusken-book)
1173 (accessed 29 January 2019).
- 1174 Whittle A, Rouse AJ, Evans JG, et al. (1993) A Neolithic Downland Monument in its Environment:
1175 Excavations at the Easton Down Long Barrow, Bishops Cannings, North Wiltshire. *Proceedings of*
1176 *the Prehistoric Society* 59. Cambridge University Press: 197–239. DOI:
1177 10.1017/S0079497X00003790.
- 1178 Zamanian K, Pustovoytov K and Kuzyakov Y (2016) Pedogenic carbonates: Forms and formation
1179 processes. *Earth-Science Reviews* 157. Elsevier B.V.: 1–17. DOI:
1180 10.1016/j.earscirev.2016.03.003.

1182 **9-Supplementary information: micromorphological descriptions,**
1183 **geochemistry scatterplots and malacological data**

Page 55 of 72

HOLOCENE									
cm	N°	Microstr. / Porosity	C-F	RD	Coarse Fraction	Micromass	BF	Org. Matter	Pedofeatures
1	64-74 70-74 N204	Complex : subangular blocky to crumbly, spongy aggregates, poorly accommodated. Moderately separated and aggregated. Prismatic secondary structure. Abundant vughs, some polyconcave. Very abundant small channels (64-70 cm).	1/20	OP	Few limestone and quartz-felds. silts to fine sands, rarely basaltic. Abundant malacoremain, several ostracods. Diatoms in micromass (64-70 cm). Several biospheroids, orthic (64-70 cm). Several <i>chara</i> oogons. Several big orthic tuffaceous concretions. (70-74 cm).	<u>-64-70 cm</u> : Yellowish to reddish brown, dark brown areas. Very organic and densely dotted and speckled. Microsparite grains. Injections of beige micromass rich in calcite and diatoms. <u>-70-74 cm</u> : Less organic, very calcitic crystallitic, even tuffaceous.	SP (top) / CC (base)	Extremely abundant small to medium fragments of reddish brown tissues (64-70 cm). Abundant micro and macrocharcoal, some millimetric (64.70 cm). Very abundant amorphous OM and organic pigment. Few small bone fragments.	Very abundant calcite fine coatings and infillings of voids. Several micritic pseudomorphs of <i>chara</i> , more abundant and more microsparitic between 70 and 74 cm. Abundant and variegated tuffaceous concretions micritic to microsparitic (especially 70-74 cm), including phytoliths and diatoms. Extremely abundant small microsparitic to sparitic nodules, better developed between 70-74 cm. Very abundant big and diffuse manganic nodules, moderately to strongly impregnated.
2									
3									
4									
5									
6									
7									
8									
9									
10									
11									
12									
13	74-79 N204+N205A	Subangular blocky to crumbly, well separated and aggregated. Abundant small channels (top and base), several vughs, some polyconcave.	1/20	OP	Few limestone silt to fine sand, few to rare quartz-felds. Few biospheroids, very abundant malacoremain, few ostracods, several <i>chara</i> oogons.	Clayey, dark brown to black, very organo-manganic, very densely dotted (obscured). Abundant microsparite grains.	CC	Very abundant microcharcoal, several to abundant macrocharcoal. Very abundant fine OM, and very abundant and variegated remains of tissues (brown, reddish brown and black).	Abundant fine calcite coatings of voids. Abundant small sparite nodules. Few injections of beige micromass from upper levels, rich in diatoms. Very abundant big brown pedogenic aggregates, very irregular, from underlying SU.
15									
16									
17									
18									
19									
20									
21									
22									
23									
24									
25									
26	79-88 N205B	Subangular to angular blocky, well separated and aggregated. Very abundant small channels, few vughs. Secondary structure roughly prismatic.	1/20	OP	Rare basaltic and scoria sands, rare volcanic minerals. Several limestone sand, few quartz-feldspar sands. Very big and abundant biospheroids, some very well-rounded. Few malacoremain and rare phytoliths.	Clayey, light brown to yellowish brown, sometimes reddish speckles. Dotted with dark particles. Microsparite grains.	CC	Abundant microcharcoal, few macrocharcoal. Abundant reddish amorphous OM remains and pigment, one bone fragment.	Very abundant and very fine calcite coatings of voids. Several small to medium sparite nodules, some small and irregular iron impregnative nodules. Few irregular and diffuse iron hypocoatings. Abundant tubular injections of micromass from upper levels (beige and rich in diatoms, black and rich in OM and charcoal).
27									
28									
29									
30									
31									
32									
33									
34									
35									
36									
37									
38									
39	88-100 N206	Subangular blocky to granular, slightly crumbly. Poorly to moderately aggregated and separated. Extremely abundant small channels (rarely bigger). Several vughs and rare chambers.	1/20	OP	Rare basaltic and scoria sands to granules, rare volcanic minerals and quartz fine sands. Several limestone medium to coarse sand. Abundant to very abundant biospheroids, few to several malacoremain, rare phytoliths.	Clayey, yellowish to greyish brown, rare reddish areas. Densely dotted with dark particles. Very abundant microsparite grains. Strong micritisation (base).	CC	Abundant to very abundant microcharcoal, several macrocharcoal, one big bone fragment. Abundant fine amorphous OM, and several brownish or reddish fragments of tissues and rootlets, several reddish spores.	Abundant very fine calcite coatings of voids, several calcite nodules, irregular to rounded, disorthic to anorthic. Several small and diffuse iron impregnative nodules, rare iron quasi-coatings of big channels. Several diffuse manganic nodules, poorly to moderately impregnated, irregular or roughly dendritic. Few to several matrix injections from upper levels (beige rich in diatoms, or black rich in OM and charcoal).
40									
41									
42									
43									
44									
45									
46									
47									
48									
49									
50									
51									
52									
53									
54									
55									
56									
57									
58									
59									
60									
61									
62									
63									
64									
65									
66									
67									
68									
69									
70									
71									
72									
73									
74									
75									
76									
77									
78									
79									
80									
81									
82									
83									
84									
85									
86									
87									
88									
89									
90									
91									
92									
93									
94									
95									
96									
97									
98									
99									
100									
101									
102									
103									
104									
105									
106									
107									
108									
109									
110									
111									
112									
113									
114									
115									
116									
117									
118									
119									
120									
121									
122									
123									
124									
125									
126									
127									
128									
129									
130									
131									
132									
133									
134									
135									
136									
137									
138									
139									
140									
141									
142									
143									
144									
145									
146									
147									
148									
149									
150									
151									
152									
153									
154									
155									
156									
157									
158									
159									
160									
161									
162									
163									
164									
165									
166									
167									
168									
169									
170									
171									
172									
173									
174									
175									
176									
177									
178									
179									
180									
181									
182									
183									
184									
185									
186									
187									
188									
189									
190									
191									
192									
193									
194									
195									
196									
197									
198									
199									
200									
201									
202									
203									
204									
205									
206									
207									
208									
209									
210									
211									
212									
213									
214									
215									
216									
217									
218									
219									
220									
221									
222									
223									
224									
225									
226									
227									
228									
229									
230									
231									
232									
233									
234									
235									
236									
237									
238									
239									
240									
241									
242									
243									
244									
245									
246									
247									
248									
249									
250									
251									
252									
253									
254									
255									
256									
257									
258									
259									
260									
261									
262									
263									
264									
265									
266									
267									
268									
269									
270									
271									
272									
273									
274									
275									
276									
277									
278									
279									
280									
281									
282									
283									
284									
285									
286									
287									
288									
289									
290									
291									
292									
293									
294									
295									
296									
297									
298									
299									
300									
301									
302									
303									
304									
305									
306									
307									
308									
309									
310									
311									
312									
313									
314									
315									
316									
317									
318									
319									
320									
321									
322									
323									
324									
325									
326									
327									
328									
329									
330									
331									
332									
333									
334									
335									
336									
337									
338									
339									
340									
341									
342									
343									
344									
345									
346									
347									
348									
349									
350									
351									
352									
353									
354									
355									
356									
357									
358									
359									
360									
361									
362									
363									
364									
365									
366									
367									
368									
369									
370									
371									
372									
373									
374									
375									
376									
377									
378									
379									
380									
381									
382									
383									
384									
385									
386									
387									
388									
389									
390									
391									
392									
393									
394									
395									
396									
397									
398									
399									
400									
401									
402									
403									
404									
405									
406									
407									
408									
409									
410									
411									
412									
413									
414									
415									
416									
417									
418									
419									
420									
421									
422									
423									
424									
425									
426									
427									
428									
429									
430									
431									
432									
433									
434									
435									
436									
437									
438									
439									
440									
441									
442									
443									
444									
445									
446									
447									
448									
449									
450									
451									
452									
453									
454									
455									
456									
457									
458									
459									
460									
461									
462									
463									
464									
465									
466									
467									
468									
469									
470									
471									
472									
473									
474									
475									
476									
477									
478									
479									
480									
481									
482									
483									
484									
485									
486									
487									
488									
489									
490									
491									
492									
493									
494									
495									
496									
497									
498									
499									
500									
501									
502									
503									
504									
505									
506									
507									
508									
509									
510									
511									
512									
513									
514									
515									
516									
517									
518									
519									
520									
521									
522									
523									
524									
525									
526									
527									
528									
529									
530									
531									
532									
533									
534									
535									
536									
537									
538									
539									
540									
541									
542									
543									
544									
545									
546									
547									
548									
549									
550									
551									
552									
553									
554									
555									
556									
557									
558									
559									
560									
561									
562									
563									
564									
565									
566									
567									
568									
569									
570									
571									
572									
573									
574									
575									
576									
577									
578									
579									
580									
581									
582									
583									
584									
585									
586									
587									
588									
589									
590									
591									
592									
593									
594									
595									
596									
597									
598									
599									
600									
601									
602									
603									
604									
605									
606									
607									
608									
609									
610									
611									
612									
613									
614									
615									
616									
617									
618									
619									
620									
621									
622									
623									
624									
625									
626									
627									
628									
629									
630									
631									
632									
633									
634									
635									
636									
637									
638									
639									
640									
641									
642									
643									
644									
645									
646									
647									
648									
649									
650									
651									
652									
653									
654									
655									
656									
657									
658									
659									
660									
661									
662									
663									
664									
665									
666									
667									
668									
669									
670									
671									
672									
673									
674									
675									
676									
677									
678									
679									
680									
681									
682									
683									
684									
685									
686									
687									
688									
689									
690									
691									
692									
693									
694									
695									
696									
697									
698									
699									
700									
701									
702									
703									
704									
705									
706									
707									
708									
709									
710									
711									
712									
713									
714									
715									
716									
717									
718									
719									
720									
721									
722									
723									
724									
725									
726									
727									
728									
729									
730									
731									
732									
733									
734									
735									
736									
737									
738									
739									
740									
741									
742									
743									
744									
745									
746									
747									
748									
749									
750									
751									
752									
753									
754									
755									
756									
757									
758									
759									
760									
761									
762									
763									
764									
765									
766									
767									
768									
769									
770									
771									
772									
773									
774									
775									
776									
777									
778									
779									
780									
781									
782									
783									
784									
785									
786									
787									
788									
789									
790									
791									
792									
793									
794									
795									
796									
797									
798									
799									
800									
801									
802									
803									
804									
805									
806									
807									
808									
809									
810									
811									
812									
813									
814									
815									
816									
817									
818									
819									
820									
821									
822									
823									
824									
825									
826									
827									
828									
829									
830									
831									
832									
833									
834									
835									
836									
837									
838									
839									
840									
841									
842									
843									
844									
845									
846									
847									
848									
849									
850									
851									
852									
853									
854									
855									
856									
857									
858									
859									
860									
861									
862									
863									
864									
865									
866									
867									
868									
869									
870									
871									
872									
873									
874									
875									
876									
877									
878									
879									
880									
881									
882									
883									
884									
885									
886									
887									
888									
889									
890									
891									
892									
893									
894									
895									
896									
897									
898									
899									
900									
901									
902									
903									
904									
905									
906									
907									
908									
909									
910									

HOLOCENE

Page 56

cm	N°	Microstr. / Porosity	C-F	RD	Coarse Fraction	Micromass	BF	Org. Matter	Pedofeatures	
1 2 3 4 5 6 7	112-124	N208	Subangular blocky to granular, poorly separated and aggregated, subangular secondary structure. Rare vughs, very abdt. small channels	1/20	OP	Rare volcanic grains, very abundant silts, some carbonated fine sands, rarely coarser. Several quartz/felds. silts, rarely fine sands. Few malacoremain and biospheroids, rare phytoliths	Clayey, greyish to yellowish brown, rarely reddish, dotted by dark particles, micritisation areas (esp. 113-114 cm), and microsparite grains	CC	Abundant microcharcoals, rare macrocharcoal, abundant fine amorphous OM. Some reddish spores. Organic pigment and abundant small reddish and brownish debris	Very fine calcite coatings of voids, several micrite hypo-coatings of channels. Several to abundant micritic to sparitic irregular nodules, orthic to disorthic, unevenly developed. Some iron quasiccoatings and hypocoatings of channels. Several very small and diffuse impregnative iron nodules. Several manganic nodules moderately to strongly impregnated, rare OM-rich matrix injections from upper horizons.
8 9 10 11 12 13 14	124-136	N209	Subangular to angular blocky well separated and aggregated. Very abundant small channels, rare vughs.	1/7	OP	Rare medium to coarse basaltic sand, well rounded. Very abundant limestone silt to coarse sand. Several to abundant quartz/felds. Silt to fine sand. Several malacoremain, few biospheroids.	Clayey, yellowish to reddish brown, with greyish areas, dotted. Microsparite grains.	CC	Abundant microcharcoal, few macrocharcoal, abundant small fragments of amorphous OM, abundant reddish pigment, abundant small reddish brown fragments of tissues.	Abundant very fine calcite coatings of voids, rarely associated with iron diffuse hypocoatings around small channels. Sometimes partial calcite infillings. Several micritic to sparitic irregular nodules, orthic to disorthic. Several orthic manganese nodules, diffuse and weakly impregnated. Rare fragments of dusty, poorly-oriented clay coatings, anorthic. Few clusters of mite droppings, linked to organic remains. Rare inclusions of OM-rich dark matrix with microcharcoal.
15 16 17 18 19 20 21 22	136-148	N210	Subangular blocky to granular, weakly separated and aggregated. Abundant small channels, some vughs, rare vesicles.	1/7	OP	Few basaltic fine to coarse sand, rare and smaller scoria, well-rounded. Rare volcanic minerals. Very abundant limestone silts to coarse sand, abundant quartz-felds. Silt to fine sand. Few malacoremain, few to several biospheroids.	Clayery, yellowish brown, some greyish or reddish areas. Dotted by dark particles. Microsparite grains.	CC to SP	Abundant microcharcoal, one big macrocharcoal. Fine amorphous OM. Rare reddish fragments from tissues and rootlets, sometimes reddish organic pugment. Two bone fragments.	Abundant very fine calcite coatings on voids, abundant middle-sized calcite nodules, microsparitic to sparitic, concentrated c. 140-142 cm, orthic to disorthic. Several very diffuse and weakly impregnated manganic nodules, typic to dendritic, very rare ferromanganic well impregnated nodules. Some diffuse micritic or manganic hypohypocoatings of porosity.
23 24 25 26 27 28 29 30 31	152-165	N211	Subangular blocky, weakly to moderately aggregated and separated, sometimes platy (base). Abundant small channels and vughs (top), but sometimes rare channels to massive (base).	1/8	OP	Few basaltic fine to coarse sand, well-rounded, and rare scoria fine sand. Very abundant limestone silt to fine sand, subangular to rounded. Abundant quartz-felds. silt to fine sand, subangular to rounded. Few biospheroid (absent at base), several malacoremain.	Clayey, yellowish brown, with greyish and reddish areas, dotted. Microsparite grains and micritisation areas (base).	CC to SP	Abundant microcharcoal, few macrocharcoal. Several fine amorphous OM and reddish organic pigment. Abundant small reddish fragments of tissues and rootlets. One bone fragment.	Abundant very fine calcite coatings of voids. Few to several micritic to sparitic calcite nodules, orthic to disorthic. Few diffuse manganic nodules, weakly to moderately impregnated. Very abundant clusters of mite droppings, associated to vegetal tissues debris.
32 33 34 35 36 37	165-172	N212A	Subangular to angular blocky, moderately to well aggregated and separated very few channels, few vughs.	1/8	OP	Several basaltic and scoria fine to medium sand, often well rounded. Abundant quartz-felds. silt to fine sand. Very abundant limestone medium to coarse sand. Rare sand-sized fragments of granite and flint. Very rare biospheroids, and several malacoremain.	Clayey, yellowish brown, greyish areas, dotted. Microsparite grains.	CC	Several microcharcoal, rare macrocharcoal. Few to several fine amorphous OM, and reddish organic pigment. Several reddish small fragments of rootlets and tissues.	Abundant fine calcite coatings of voids. Rare laminated calcite coatings of coarse particles, anorthic. Rare sparitic calcite nodules, anorthic. Abundant tuffaceous concretions remains (tubes), anorthic. Rare diffuse manganic nodules. One dusty clay coating fragment, anorthic. Some big clayey pedogenic aggregates, elongated and with diffuse borders, with striated BF (crust), anorthic. Abundant clusters of mite droppings, associated to organic debris.

HOLOCENE									
cm	N°	Microstr. / Porosity	C-F	RD	Coarse Fraction	Micromass	BF	Org. Matter	Pedofeatures
1	166-178	N212B	Single-grain (base, sand); intergrain microaggregate (middle); blocky (top). Well separated, not aggregated.	9/10	CP (top) /EG/ MG (base)	Sand: Several small scoria, abundant basalt, abundant quartz and feldspar, extremely abundant and coarse limestone grains, some sparite fragments. Several small volcanic minerals (olivine, pyroxene, nepheline). Few flint and rare granite grains. Several malacoremain, very abundant biospheroids well-rounded and with micrite coatings.	If present, clayey, yellowish brown, dotted, microsparite grains.	CC (top)	Rare microcharcoal, few macrocharcoal, rare fine amorphous OM. Few Reddish fragments of tissues. Few to several small to medium-sized bone fragments. Calcite coatings of most sand grains, sometimes polyphased (pisolithe-like), anorthic. Few <i>chara</i> pseudomorphs, anorthic. Several well-rounded sparitic nodules, anorthic. Several pedosedimentary fragments of clay infillings/coatings with variegated features. Some reddish to dark brown pedosedimentary aggregates.
2									
3									
4									
5									
6									
7									
8	178-186	N213	Fissural structure to subangular blocky, very poorly separated and aggregated. Intrapedal massive, rare vughs.	3/4	CP /SSP	Several basaltic and scoria fine to coarse sand, well-rounded. Several volcanic minerals including nepheline. Several quartz-felds. sand. Few small fragments of flint, and rare of granite. Extremely abundant limestone fine sand to granules, several sparite fragments. Abundant fragmented malacoremain, roughly bedded. Several well-rounded biospheroids.	Clayey, yellowish to greyish brown, dotted. Microsparite grains.	CC	Abundant microcharcoal, several to abundant macrocharcoal. Rarely reddish organic pigment and fine amorphous OM. Few reddish fragments of tissues and rootlets, several bone fragments (up to 3 mm) Rare fine calcite coatings of voids. Few small sparitic nodules, orthic. Abundant microlaminated micritic coatings of sands, pisolith-like (top). Few organo manganic nodules, strongly impregnated. Few mite droppings. Some well-rounded anorthic pedosedimentary aggregates, with variegated characteristics. Rare tube-like tuffaceous concretions, anorthic.
9									
10									
11									
12									
13									
14									
15	188-195	N214	Single-grain (top, sand), to fissural (base) Well separated, not aggregated (base)	¾ to 1/5 (base)	MG (top)/ CP/ OP (base)	Abundant basaltic coarse sand, few scoria. Several to abundant volcanic minerals (nepheline, analcime). Several quartz/felds. fine to coarse sand, and extremely abundant limesto fine to coarse sand. Abundant sparite crystals, and some tube-like tuffaceous concretions. Rare small flint fragments. Several to abundant fragmented malacoremain, and several biospheroids, well-rounded.	If present, clayey, yellowish to greyish brown, finely doted, microsparite grains.	CC (base)	Several microcharcoal, few to several macrocharcoal. Fine amorphous OM. Some reddish fragments from rootlets and tissues. Several small to medium-sized bone fragments. Few fine calcite coatings of voids, few calcite nodiles, some well-rounded. Microlaminated calcite coatings of some mineral or biomineral grains (orthic). Few small pedosedimentary fragments of clay coatings or infillings. Few pedosedimentary aggregates with variegated features, well-rounded. Few small and diffuse iron and manganic nodules, weakly impregnated.
16									
17									
18									
19									
20									
21									
22									
23									
24									
25									

Table 3: Micromorphological description of NAR2 by thin section. C-F: Coarse-Fine. RD: Related Distribution, (OP: Open Porphyric, CP: Closed Porphyric, SSP: Single Spaced Porphyric, MG: Monic, EG: Enaulic). BF: Birrefringence Fabric (SP: Speckled, CC: Calcitic Cristallitic).

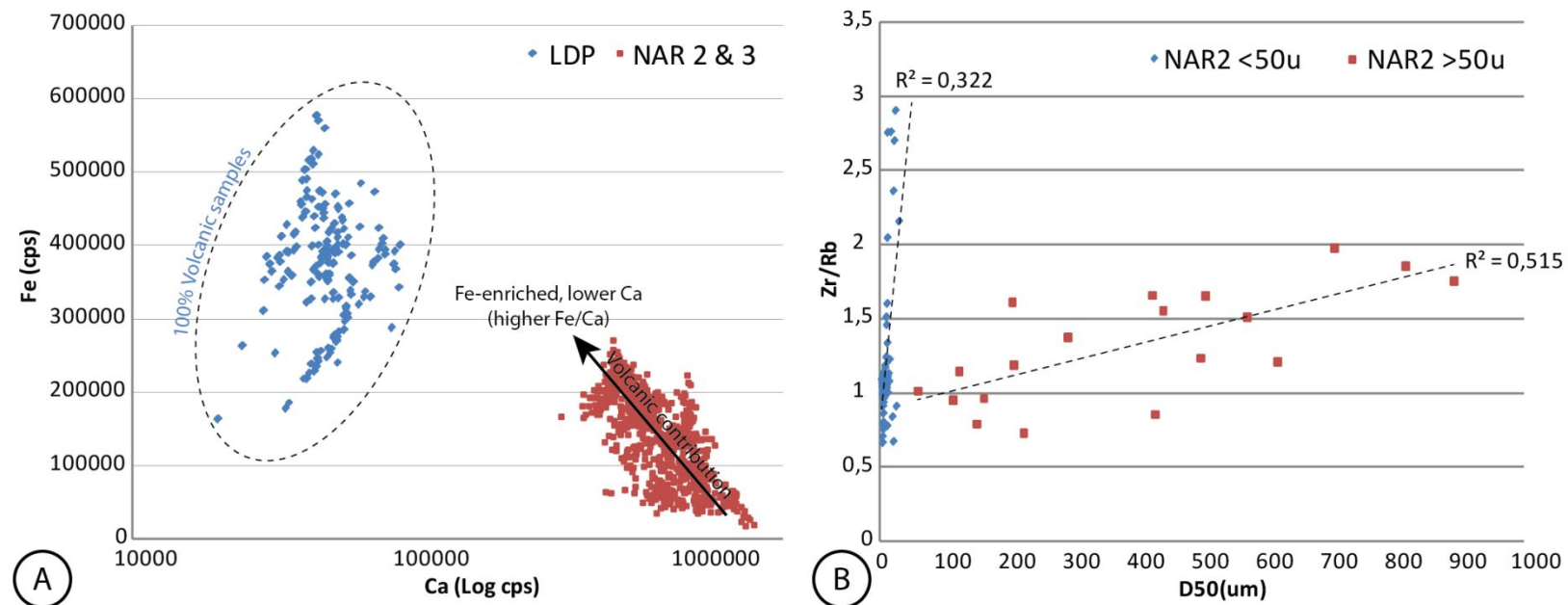


Figure 12. A) Scatterplot showing relative contents in Fe and Ca (measured by XRF core-scanner in cps, Log scale for Ca) of 100% volcanic samples (LDP blue dots, core from the summit of the Puy de Corent, lithology: basalts and scoria, data from Mayoral, 2018), vs. samples from NAR2 & NAR3 in the calcareous lowlands (this study, red dots). 100% volcanic samples have clearly higher Fe/Ca ratio. Note also the gradient in the Fe/Ca ratio for NAR2 & NAR3 samples interpreted as increased volcanic sediment content. B) Scatterplot showing relationship between Zr/Rb ratio and D50 in NAR2 samples, for two different grain-size classes. Zr/Rb is very sensitive to grain-size increase in clays and fine to coarse silts (<50um, blue dots), and moderately sensitive for very coarse silts and sands (>50um, red dots). Note that relatively low R^2 is mainly due to the reduced number of samples.

1		Sedimentary subunit	2.24	2.23	2.22	2.21	2.20	2.19	2.18	2.17	2.16 inf	2.16 sup	2.15	2.14	2.13	2.12	2.11	2.10	2.9
2		Depth (cm)	196-202	194-196	186-194	180-184	170-178	164-170	158-162	154-158	142-154	132-142	122-132	114-122	100-114	90-100	86-90	80-84	70-78
3		<i>Arianta arbustorum</i>	1	4	2	1	2	1		1	1	1	1	1	1	1			
4		<i>Clausilia</i> sp.		1	2	1	1	1		1									
5	F	<i>Discus rotundatus</i>			1		1												
6		<i>Pomatias elegans</i>	1	1	5	4	2	1			1	1							
7		<i>Cochlicopa lubrica</i> agg.	5	4	6	6	3	3	1	1	11	9	6	7	2	2			1
8		Slugs	22	6	17	1	7	3	1	1	6	1	5	5	2	2		1	2
9		<i>Nesovitrea hammonis</i>		1															
10	M	<i>Punctum pygmaeum</i>		1	1							1	2						
11		<i>Trochulus hispidus</i>				2	1					1	6	3	8	1	5	2	
12		<i>Vallonia costata</i>	6	5	5	4	4	2		2	2	6	3	4	5	6	7	4	5
13		<i>Carychium minimum</i>					1					15	34	59	10			1	
14		<i>Oxyloma elegans</i>	9	2	7		3	3	1	1	2	15	4	10	6	3	1		2
15	P	<i>Vertigo angustior</i>	2	1		1													
16		<i>Vertigo antivertigo</i>	7						1		1	8	11	14					
17		<i>Zonitoides nitidus</i>	3	2								1	1	1					
18		<i>Chondrula tridens</i>		1	1		1												
19		<i>Helicella itala</i>	2		14		1	2	1	3	3	2			1	1	1		2
20		<i>Pupilla muscorum</i>	9	10	9	5	4	2	1	1	5	2	1		1	1	3	1	1
21	O	<i>Vallonia excentrica</i>	17	3	5	8		6							6	19	23	5	
22		<i>Vallonia pulchella</i>		8	13		10	6	5	9	46	154	39	77	14	11			7
23		<i>Vertigo pygmaea</i>		2	4	2			4	1	7	5	1	4	3	4	2	4	4
24		<i>Acroloxus lacustris</i>																	4
25		<i>Ancylus fluviatilis</i>		1															
26		<i>Anisusleucostoma</i>	4		2	1		4	4	1	2	13	39	65	28	2			7
27		<i>Galba truncatula</i>	11	10				2	1	2	19	79	15	18	17				3
28		<i>Gyraulus albus</i>	1	1	2	1			1	1			1	2	6	1			4
29		<i>Gyraulus crista</i>	19	12	7				1				2	3	5	1	1	2	57
30	A	<i>Hippeutis complanatus</i>											1	3	4				8
31		<i>Lymnaea stagnalis</i>	1																
32		<i>Physa fontinalis</i>											2	2	2				2
33		<i>Pisidium</i> sp.	27	16	32	16	10	19	11	2	2	1	5	8	4				3
34		<i>Radix balthica</i>	20	8	1	4	3	7	3			21	10	4	5	1			11
35		<i>Valvata cristata</i>													1				1
36		Count	167	100	136	57	54	62	36	27	108	334	183	295	120	50	35	41	131
37		<i>Cecilioides acicula</i>									3								
38																			

Table 4: Fauna list of malacological samples from NAR2 core. Species are classified by ecological affinities (F : forested environment; M : mesophilic species ; P : palustrine environment ; O : open environment ; A : aquatic species) and by alphabetical order.

1

2

3

4

5

6

7

8

9

10

11

12

13

14

15

16

17

18

19

20

21

22

23

24

25

26

27

28

29

30

31

32

33

34

35

36

37

38

39

40

41

42

43

44

45

46

	Sedimentary subunit	3.13	3.12			3.11		3.10	3.9			3.8		3.7	3.6	
		193-201	187-193	181-187	174-181	165-171	159-165	147-156	140-147	134-140	128-134	120-128	114-120	104-112	92-103	84-92
	Depth (cm)															
F	<i>Arianta arbustorum</i>		1	1	1	3	2	9	1	1	1	1	1	1		
	<i>Clausilia</i> sp.								1							
	<i>Pomatias elegans</i>				1	1						1				
	<i>Cochlicopa lubrica</i> agg.			3	4	10	12	29	16	11	7	5	5	5	3	3
	Slugs	6	4	13	20	32	29	75	59	38	21	25	16	12	4	2
M	<i>Nesovitrea hammonis</i>		1			2	1	4	2							
	<i>Punctum pygmaeum</i>				1		1	2	1	1			2			
	<i>Trochulus hispidus</i>								1			2	5	1	5	1
	<i>Vallonia costata</i>	3		6	7	11	7	35	12	6	1	3				
	<i>Vitrina pellucida</i>				1	1	1									
	<i>Carychium minimum</i>		1	4	10	28	32	25	3	2			4	16	1	
	<i>Oxyloma elegans</i>	1			8	11	14	44	24	15	15	10	9	18	18	6
	<i>Vertigo angustior</i>			1	4	9	16	4	1				1	1		
P	<i>Vertigo antivertigo</i>	2		5	11	20	31	22	8	10	2	2	5	21	5	
	<i>Vertigo moulinsiana</i>							1								
	<i>Zonitoides nitidus</i>			1	2	4	6	1						4	8	
	<i>Helicella itala</i>		8		1		3	12	8	16	2	9	5	4		
	<i>Pupilla muscorum</i>	3	5	6	2	7	7	29	36	21	8	7	10	7		
O	<i>Vallonia excentrica</i>								15	8						
	<i>Vallonia pulchella</i>	20	55	73	102	100	126	202	252	182	44	23	104	95	18	15
	<i>Vertigo pygmaea</i>		6	4	8	17	19	20	29	22	4	6	23	11	2	
	<i>Acroloxus lacustris</i>														6	12
	<i>Anisus leucostoma</i>					3		2	1	2	1		4	16	34	
	<i>Galba truncatula</i>	1		3	14	28	21	7	6	32	24	9	28	57	48	17
	<i>Gyraulus albus</i>														13	31
	<i>Gyraulus crista</i>				3	9	3	2	3	1	2			1	74	112
	<i>Hippeutis complanatus</i>														9	9
A	<i>Lymnaea stagnalis</i>															2
	<i>Physa fontinalis</i>														8	
	<i>Pisidium</i> sp.	2	1	1	1	5	4	2					2	18	35	13
	<i>Planorbis planorbis</i>	1		1					1					13	26	26
	<i>Radix balthica</i>					4	1						2	18	27	22
	<i>Radix labiata</i>	1	4	3	10	23	36	45	39	21	2					
	<i>Valvata cristata</i>														2	14
	Count	40	86	125	211	328	372	572	519	389	134	103	226	319	346	285
	<i>Cecilioides acicula</i>			1					1	1	1					

Table 5: Fauna list of malacological samples from NAR3 core. Species are classified by ecological affinities (F : forested environment; M : mesophilic species ; P : palustrine environment ; O : open environment ; A : aquatic species) and by alphabetical order. Grey columns indicate samples which were grouped in order to reach a number in accordance with the representativeness threshold of Evans (1972)

1
2
3
4
5
6
7
8
9
10
11
12
13
14
15
16
17
18
19
20
21
22
23
24
25
26
27
28
29
30
31
32
33
34
35
36
37
38
39
40
41
42
43
44
45
46
47
48
49
50
51
52
53
54
55
56
57
58
59
60

1204

Accepted Manuscript

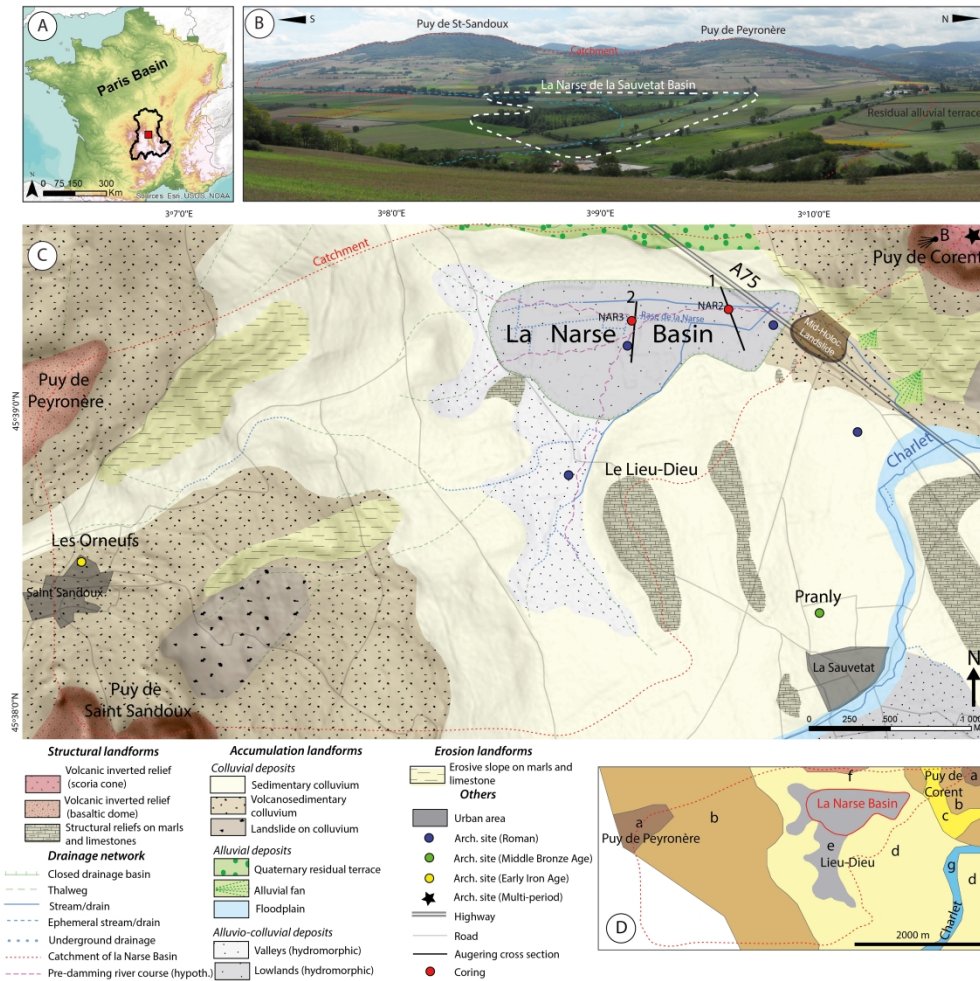


Figure 1. A) Location of study area, black line delineates Auvergne region; B) General view of study area from the summit of the Puy de Corent (location: see Fig. 1C, view direction: ESE). La Narse hydromorphic basin and its catchment are indicated with white and red dashed lines respectively. Light blue dashed line indicates hypothetical position of former river course (Pleistocene and Early Holocene), from cross sections and current topography (see Mayoral et al., 2018); C) Geomorphological sketch of la Narse de la Sauvetat catchment (modified from Mayoral et al., 2018) ; D) Main soils of the catchment (red dashed line) following Bornand et al., 1968 : a) lithosols and brown soils on basalts ; b) Calcareous and calcic brown soils on marls and basaltic colluvium ; c) Colluvial soils and regosols on marls and platy limestone ; d) Calcareous brown soils on gentle slopes ; e) Clayey grey soils of marly depressions, hydromorphic and isohumic; f) Calcareous brown soils from thin residual terraces ; g) Gleyic soils from clayey alluvium of streams and marly lowlands.

410x405mm (300 x 300 DPI)

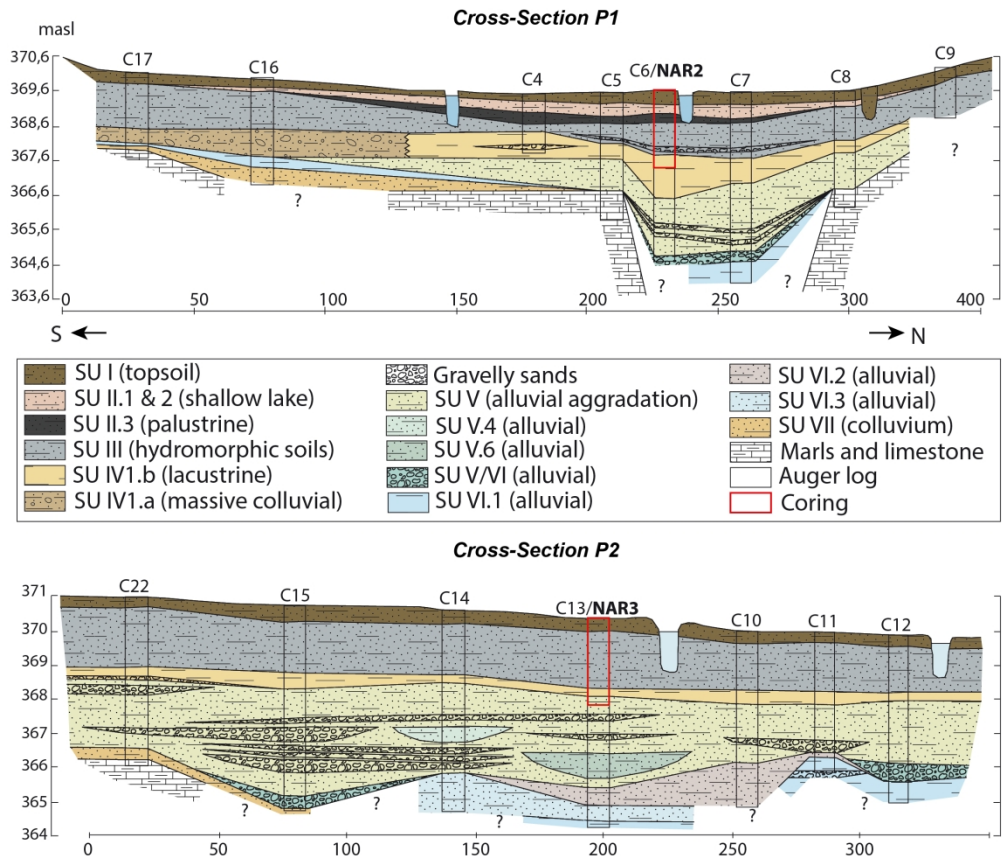


Figure 2. Selected stratigraphic cross-sections of the basin (P1 and P2, adapted from Mayoral et al., 2018) with location of cores NAR2 and NAR3 (see also Fig. 1C).

210x181mm (300 x 300 DPI)

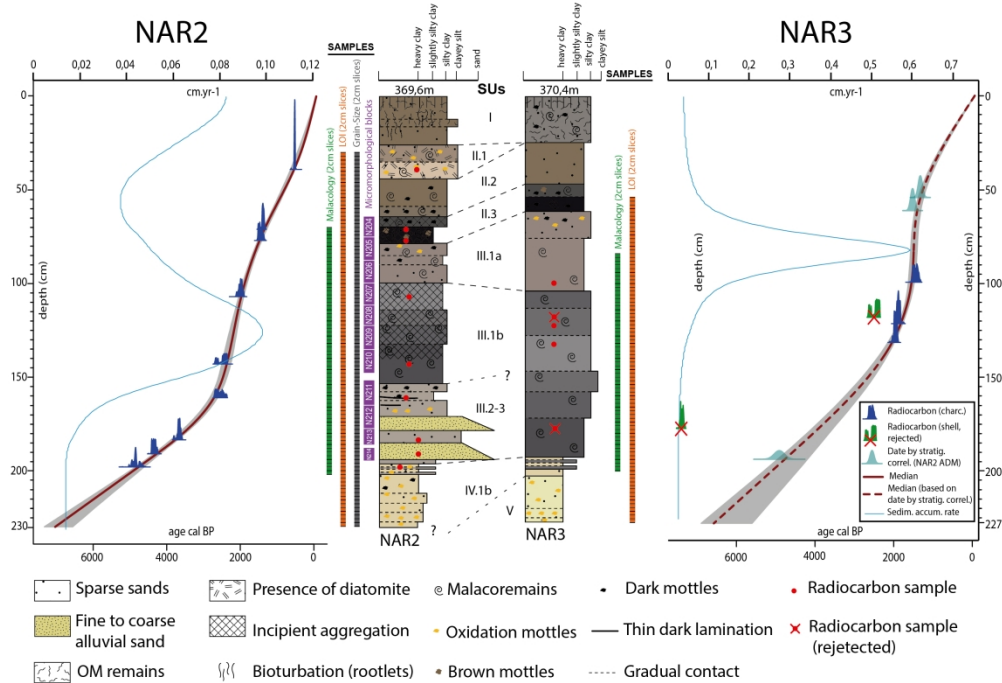


Figure 3. Litho-stratigraphy, stratigraphic correlations, sampling and age-depth model of NAR2 (left) and NAR3 (right) cores.

242x168mm (300 x 300 DPI)

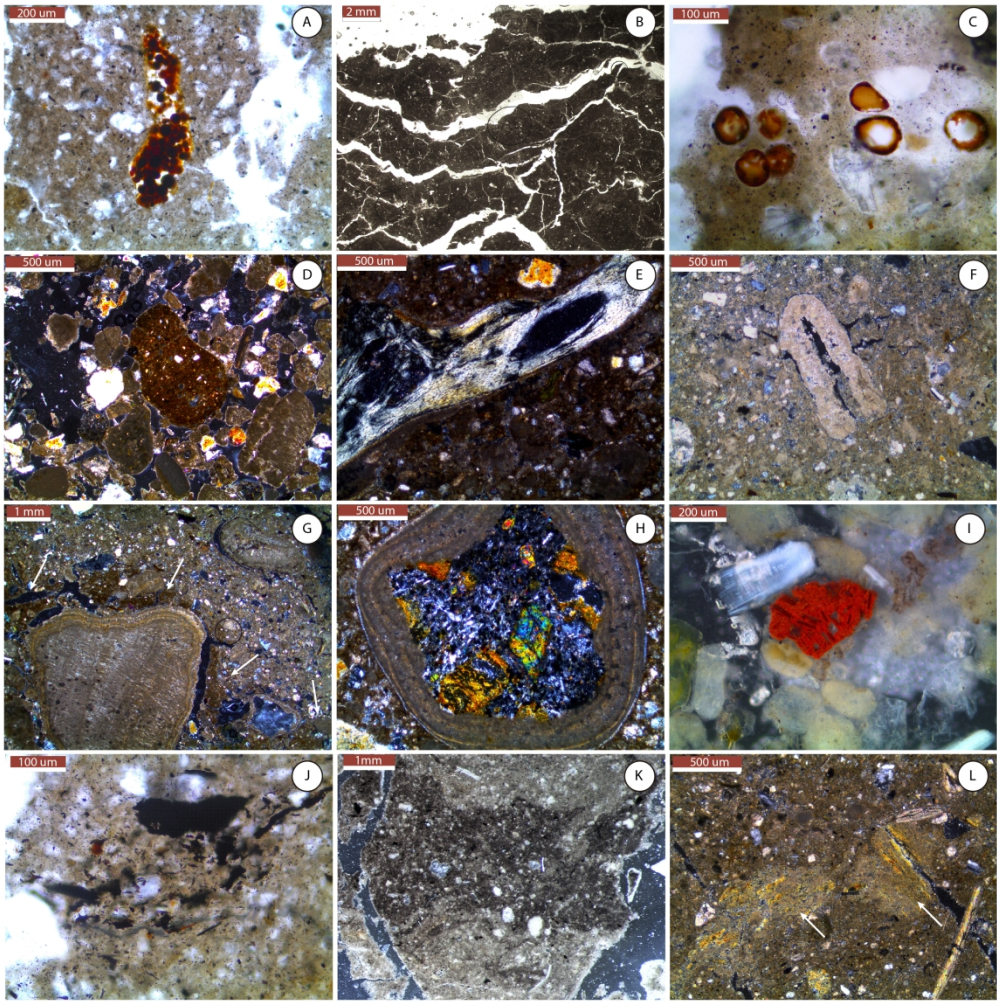


Figure 4. Selected micromorphological features of lower NAR2 (Micromorphological Units MVII to MIV, see text and Fig. 6). A) Cluster of mite droppings, microcharcoal-rich micromass (MIV, N211, PPL-Plane Polarized Light). B) Platy microstructure (MIV, N211, transmitted light). C) Spore remains (MIV, N211, PPL). D) Rounded pedosedimentary aggregate (reddish matrix), surrounded mainly by carbonated micritic sands (MV, N212B, XPL-Crossed Polarized Light). E) Bone fragment (MVI, N213, XPL). F) Fragment of micritic to micro-sparitic carbonated root concretion (MIV, N212A, XPL). G) Contact (arrows) of coarse sands with silty clays. Note the big stromatolitic/tuffaceous fragment of limestone, with a secondary microlaminated calcite coating (MV, N212B, XPL). H) Fragment of basalt with a coating of microlaminated calcite (micrite and microsparite) and rounded by transport (MVI, N213, XPL). I) Volcanic reddish scoria fragment, including translucent plagioclases (MV, N212B, OIL-Oblique Incident Light). J) Cluster of charcoal and in-situ charred remains (MIV, N211, PPL). K) Portion of dark matrix, with more abundant coarse fraction, more humic and enriched in microcharcoal, probably from a surficial soil horizon (MIV, base of N211, OIL). L) Clayey aggregates with striated B-Fabric (arrows), likely degraded fragments of slaking crust (MIV, N212A, XPL).

286x288mm (300 x 300 DPI)

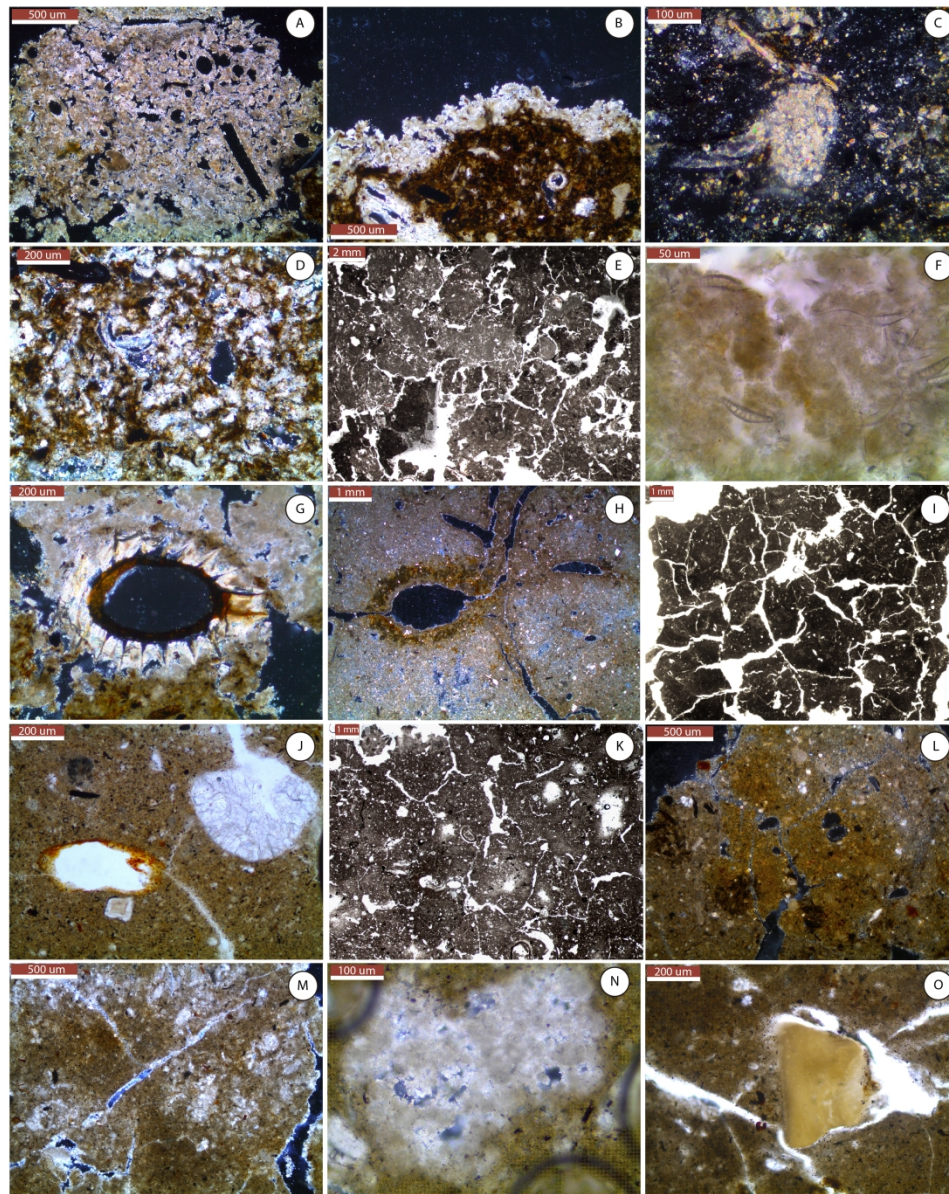
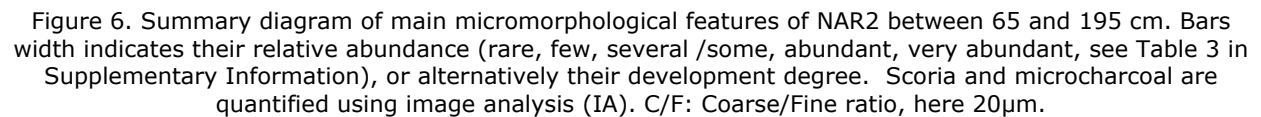


Figure 5. Selected micromorphological features from upper NAR2 (Micromorphological Units MIII to MI, see text and Fig.6). A) Orthitic tuffaceous concretion, from aggregation of smaller micritic elements and pseudomorphs (MI, N204, XPL-Crossed Polarized Light). B) Tuffaceous calcite capping. Note dark micromass, rich in organic matter (MI, N204, XPL). C) Orthitic calcite nodule in a dark crystalline to isotropic micromass (MI, N204, XPL). D) Micromass rich in calcitic grains strongly bioturbated and reorganized by biological activity (MI, N204, XPL). E) Complex microstructure, subangular with granular substructure or crumbly subangular (MI, N204, transmitted light). F) Diatoms embedded in carbonate-rich micromass (MI, N204, PPL-Plane Polarized Light). G) Characeae oogon. Note the two different types of micromass: brown, clayey, rich in organic fragments and microcharcoal (base) vs. massive micritic-microsparitic micromass (top) (MI, N204, XPL). H) Iron and micritic hypocoatings around a chamber and fissural to canalicular voids (MIII, N208, XPL). I) Subangular blocky microstructure of an organo-mineral unit (MIII, N207, transmitted light). J) Iron hypocoating and biospheroid, note silty clay micromass rich in microcharcoal and small organic fragments (MII, N205, PPL). K) Granular microstructure of an organo-mineral unit, note partial collapse of porosity due to secondary clogging (MIII, N210, transmitted light). L) Silty clay matrix highly impregnated

1
2
3
4
5
6
7
8
9
10
11
12
13
14
15
16
17
18
19
20
21
22
23
24
25
26
27
28
29
30
31
32
33
34
35
36
37
38
39
40
41
42
43
44
45
46
47
48
49
50
51
52
53
54
55
56
57
58
59
60

by oxidized iron, and injection of matrix aggregates (rich in organic matter) from upper layers (MII, N205, XPL). M) Concentration of micritic to microsparitic calcite in the matrix (and in voids), some evolving to nodules (MIII, N208, XPL). N) Calcite nodule (micritic to microsparitic) in development by impregnation of the matrix (MIII, N209, XPL). O) Small bone fragment embedded in a silty clay matrix with microcharcoal and organic microdebris (MII, N205, PPL).

286x358mm (300 x 300 DPI)



<http://mc.manuscriptcentral.com/holocene>

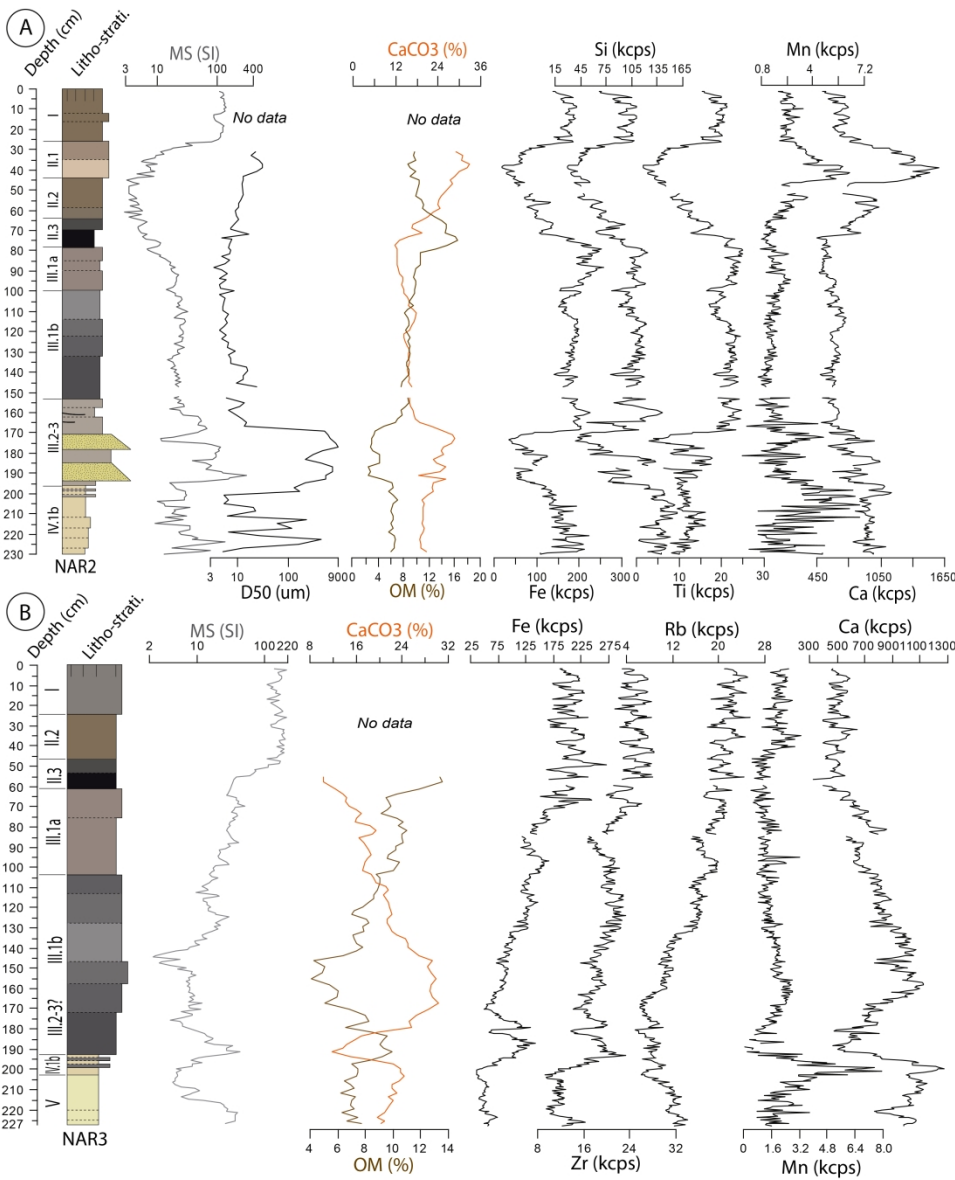


Figure 7. A) Selected elements and sedimentological data for NAR2. Values are in 10⁻⁵ SI (Magnetic Susceptibility-MS-) and in counts per second (CPS) for the XRF. B) Selected elements and sedimentological data for NAR3.

323x404mm (300 x 300 DPI)

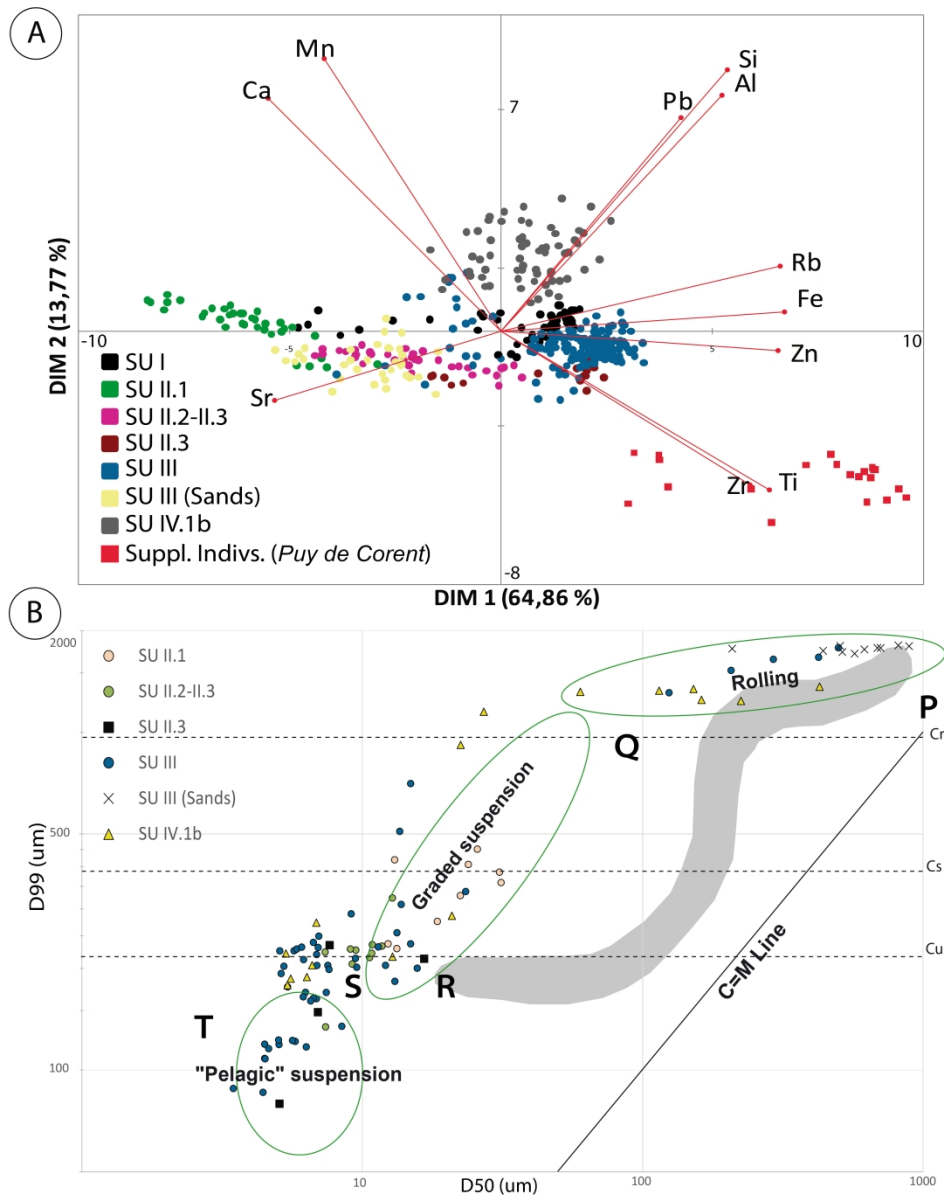


Figure 8. A) PCA biplot of selected geochemical variables according to dimensions 1 and 2, individuals are distributed by Sedimentary Unit. Note supplementary individuals (red squares, data from Mayoral et al., 2018). B) Passega or C-M diagram of NAR2 with grain-size data by Sedimentary Unit. Grey area represents reference C-M diagram by Passega (1977).

323x404mm (300 x 300 DPI)

1
2
3
4
5
6
7
8
9
10
11
12
13
14
15
16
17
18
19
20
21
22
23
24
25
26
27
28
29
30
31
32
33
34
35
36
37
38
39
40
41
42
43
44
45
46
47
48
49
50
51
52
53
54
55
56
57
58
59
60

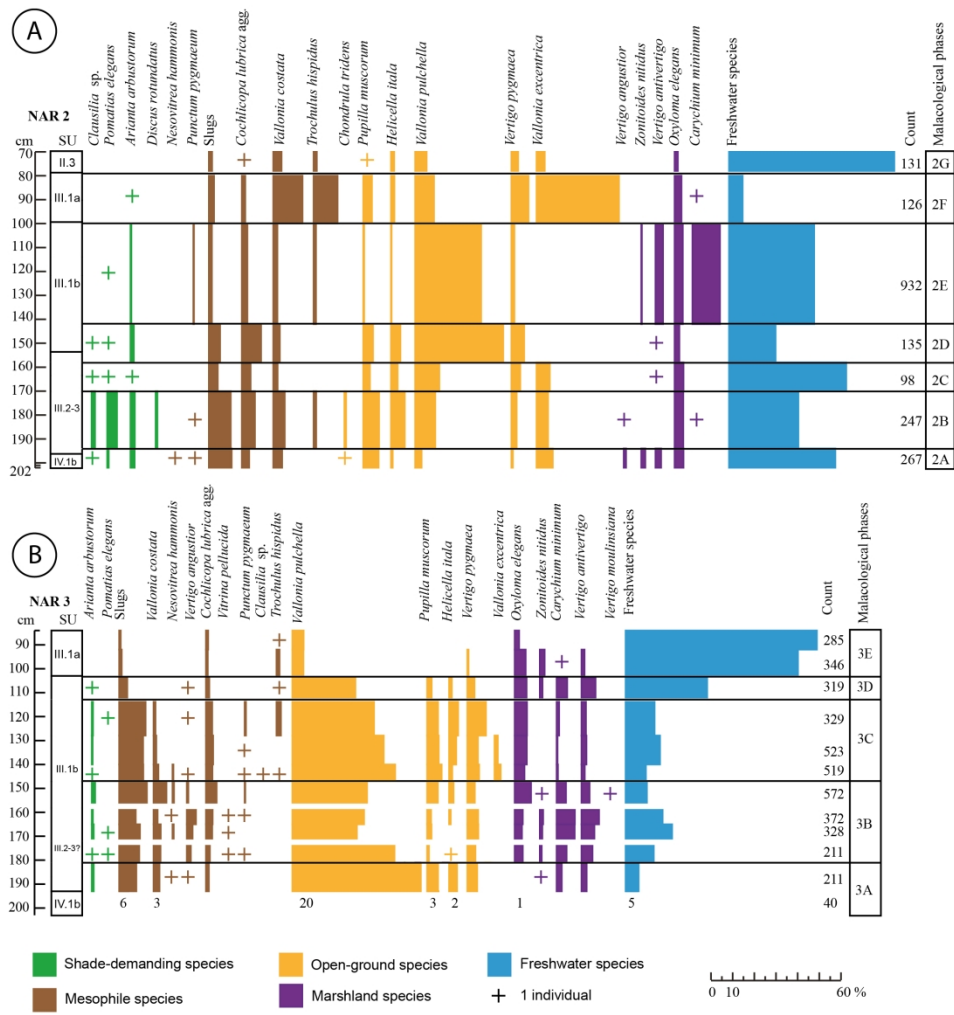
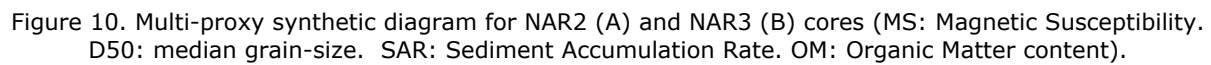


Figure 9. Diagrams of specific composition of molluscan assemblages A) NAR2 B) NAR3. Contiguous 2cm-thick sediment samples were grouped in bigger sets when necessary in order to reach a significant number of shells. Species are classified by ecological affinities and by order of occurrence.

210x216mm (300 x 300 DPI)



<http://mc.manuscriptcentral.com/holocene>

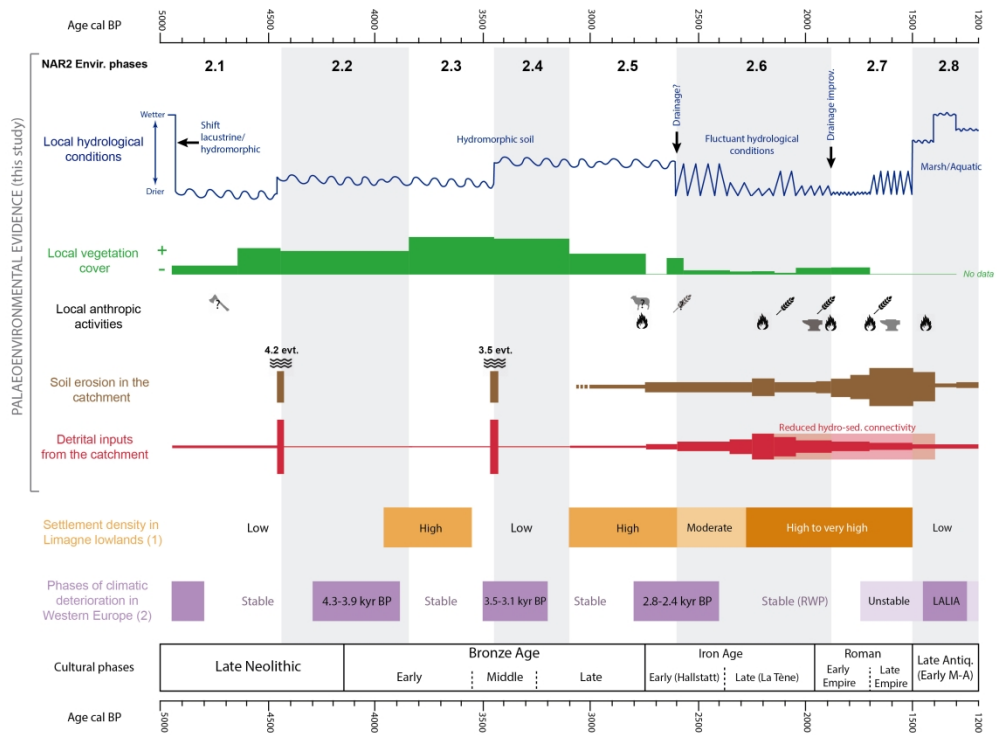


Figure 11. Comparison of palaeoenvironmental evidence in la Narse de la Sauvetat between 5000 and 1200 cal BP (derived from core NAR2, this study) with regional archaeological data in Limagne plain and climatic changes in Western Europe. NAR2 environmental phases are from Fig. 10A. Representations of local hydrological conditions, soil erosion in the catchment and detrital inputs are qualitative (relative level or thickness according to process intensity) and based on data from Fig. 10. High-energy hydro-sedimentary episodes related to 4.2 and 3.5 kyr. cal BP climatic events are indicated (note a chronological offset of 150-200 yr. of the first episode, see the text for details). Local vegetation cover (qualitative) is represented by the proportion of shade-demanding malacological species vs. other terrestrial malacological species. Anthropic activities (landscape opening, use of fire, pastoral activity, agriculture and metallurgical activity) are represented by symbols. RWP: Roman Warm Period. LALIA: Late Antiquity Little Ice Age. Settlement density in Limagne is based on (1) Ballut and Argant, 2004; Couderc, 2019; Daugas and Raynal, 1989; Milcent and Mennessier-Jouannet, 2007; Raynal et al., 2003; Trément et al., 2007; Trément, 2011. Phases of climatic deterioration in Western Europe are based on (2) Berger et al., 2007; Brisset et al., 2013; Buntgen et al., 2011; Carozza et al., 2015; Fletcher, Debret and Goñi, 2013; Holzhauser et al., 2005; Joerin et al., 2006; Magny, 2004; Magny et al., 2009; McCormick et al., 2012; Van Geel and Magny, 2002; Walker et al., 2019; Walsh et al., 2019.

282x207mm (300 x 300 DPI)

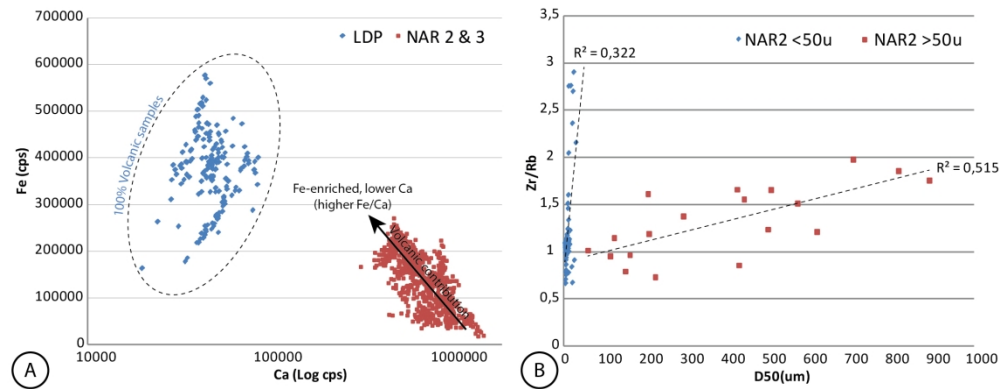


Figure 12. A) Scatterplot showing relative contents in Fe and Ca (measured by XRF core-scanner in cps, Log scale for Ca) of 100% volcanic samples (LDP blue dots, core from the summit of the Puy de Corent, lithology: basalts and scoria, data from Mayoral, 2018), vs. samples from NAR2 & NAR3 in the calcareous lowlands (this study, red dots). 100% volcanic samples have clearly higher Fe/Ca ratio. Note also the gradient in the Fe/Ca ratio for NAR2 & NAR3 samples interpreted as increased volcanic sediment content. B) Scatterplot showing relationship between Zr/Rb ratio and D50 in NAR2 samples, for two different grain-size classes. Zr/Rb is very sensitive to grain-size increase in clays and fine to coarse silts (<50um, blue dots), and moderately sensitive for very coarse silts and sands (>50um, red dots). Note that relatively low R2 is mainly due to the reduced number of samples.

185x73mm (300 x 300 DPI)